Pancreatic β-cell tRNA hypomethylation and fragmentation link TRMT10A deficiency with diabetes.

Cristina Cosentino, Sanna Toivonen, Esteban Diaz Villamil, Mohamed Atta, Ravanat Jean-Luc, Stéphane Demine, Andrea Alex Schiavo, Nathalie Pachera, Jean-Philippe Deglasse, Jean-Christophe Jonas, et al.

▶ **To cite this version:**

Cristina Cosentino, Sanna Toivonen, Esteban Diaz Villamil, Mohamed Atta, Ravanat Jean-Luc, et al.. Pancreatic β-cell tRNA hypomethylation and fragmentation link TRMT10A deficiency with diabetes.. Nucleic Acids Research, 2018, 46 (19), pp.10302-10318. 10.1093/nar/gky839 . hal-01945851

HAL Id: hal-01945851
https://hal.science/hal-01945851

Submitted on 4 Jun 2024

HAL is a multi-disciplinary open access archive for the deposit and dissemination of scientific research documents, whether they are published or not. The documents may come from teaching and research institutions in France or abroad, or from public or private research centers.

L'archive ouverte pluridisciplinaire **HAL**, est destinée au dépôt et à la diffusion de documents scientifiques de niveau recherche, publiés ou non, émanant des établissements d'enseignement et de recherche français ou étrangers, des laboratoires publics ou privés.

10302–10318 *Nucleic Acids Research, 2018, Vol. 46, No. 19* *Published online 21 September 2018*
doi: 10.1093/nar/gky839

Pancreatic β-cell tRNA hypomethylation and fragmentation link TRMT10A deficiency with diabetes

Cristina Cosentino[1,†], Sanna Toivonen[1,†], Esteban Diaz Villamil[1], Mohamed Atta[2], Jean-Luc Ravanat[3], Stéphane Demine[1], Andrea Alex Schiavo[1], Nathalie Pachera[1], Jean-Philippe Deglasse[4], Jean-Christophe Jonas[4], Diego Balboa[5], Timo Otonkoski[5,6], Ewan R. Pearson[7], Piero Marchetti[8], Décio L. Eizirik[1], Miriam Cnop[1,9,*] and Mariana Igoillo-Esteve[1,*]

[1]ULB Center for Diabetes Research, Université Libre de Bruxelles, 1070 Brussels, Belgium, [2]CEA/Grenoble, DRF/BIG/LCBM UMR5249, Grenoble, France, [3]Université Grenoble Alpes, CEA, CNRS INAC, SyMMES UMR 5819, Grenoble, France, [4]Université Catholique de Louvain, Institut de Recherche Expérimentale et Clinique, Pôle d' Endocrinologie, Diabète et Nutrition, Brussels, Belgium, [5]Research Programs Unit, Molecular Neurology and Biomedicum Stem Cell Centre, Faculty of Medicine, University of Helsinki, Helsinki, Finland, [6]Children's Hospital, University of Helsinki and Helsinki University Hospital, Helsinki, Finland, [7]Division of Cardiovascular and Diabetes Medicine, Medical Research Institute, Ninewells Hospital and Medical School, Dundee, UK, [8]Department of Clinical and Experimental Medicine, University of Pisa, Pisa, Italy and [9]Division of Endocrinology, Erasmus Hospital, Université Libre de Bruxelles, 1070 Brussels, Belgium

Received March 31, 2018; Revised August 17, 2018; Editorial Decision September 05, 2018; Accepted September 10, 2018

ABSTRACT

Transfer RNAs (tRNAs) are non-coding RNA molecules essential for protein synthesis. Post-transcriptionally they are heavily modified to improve their function, folding and stability. Intronic polymorphisms in *CDKAL1*, a tRNA methylthiotransferase, are associated with increased type 2 diabetes risk. Loss-of-function mutations in *TRMT10A*, a tRNA methyltransferase, are a monogenic cause of early onset diabetes and microcephaly. Here we confirm the role of TRMT10A as a guanosine 9 tRNA methyltransferase, and identify $tRNA^{Gln}$ and $tRNA^{iMeth}$ as two of its targets. Using RNA interference and induced pluripotent stem cell-derived pancreatic β-like cells from healthy controls and TRMT10A-deficient patients we demonstrate that TRMT10A deficiency induces oxidative stress and triggers the intrinsic pathway of apoptosis in β-cells. We show that tRNA guanosine 9 hypomethylation leads to $tRNA^{Gln}$ fragmentation and that 5′-$tRNA^{Gln}$ fragments mediate TRMT10A deficiency-induced β-cell death. This study unmasks tRNA hypomethylation and fragmentation as a hitherto unknown mechanism of pancreatic β-cell demise relevant to monogenic and polygenic forms of diabetes.

INTRODUCTION

tRNAs are non-coding RNA molecules essential for protein synthesis. After transcription, tRNAs undergo nuclear maturation involving 5′ leader sequence removal, 3′ trailer trimming, CCA addition, intronic splicing, and post-transcriptional modifications that modulate their function, folding and stability (1,2). More than 90 different tRNA modifications have been described in mammals. These modifications are introduced by nuclear, cytosolic or mitochondrial tRNA-modifying enzymes. Up to 20% of cytoplasmic tRNA nucleosides are modified, most often by methylation (2). The biological role of most tRNA modifications remains unknown. Modifications in or around the anticodon (at positions 34 and 37) play an important role in decoding accuracy and maintenance of the reading frame (3–5). Modifications within the tRNA body modulate tRNA folding, stability and amino-acylation (2,6). tRNAs are among the most stable RNA species *in vivo*, but reduced tRNA modifications may lead to their degradation (7–9) or fragmentation by endonucleases (10). Angiogenin-mediated cleavage at the anticodon generates 29–50 nucleotide-long 5′- and 3′-tRNA halves also called tRNA-derived stress-

*To whom correspondence should be addressed. Tel: +32 2 555 6138; Email: migoillo@ulb.ac.be
Correspondence may also be addressed to Miriam Cnop. Tel: +32 2 555 6305; Email: mcnop@ulb.ac.be
†The authors wish it to be known that, in their opinion, the first two authors should be regarded as Joint First Authors.

© The Author(s) 2018. Published by Oxford University Press on behalf of Nucleic Acids Research.
This is an Open Access article distributed under the terms of the Creative Commons Attribution Non-Commercial License (http://creativecommons.org/licenses/by-nc/4.0/), which permits non-commercial re-use, distribution, and reproduction in any medium, provided the original work is properly cited. For commercial re-use, please contact journals.permissions@oup.com

induced RNAs (tiRNAs) (10–12). Shorter tRNA fragments (tRFs) of 14–30 nucleotides are generated by Dicer, Dgcr8 (13) and possibly other endonucleases (14). tRNA fragmentation is a stress-regulated process that is positively or negatively tuned by the presence of tRNA modifications (15–17). Extensive human genetic evidence has linked loss-of-function mutations in tRNA-modifying enzymes with cancer, neurological disorders, mitochondrial disease and diabetes (10,18). Mitochondrial tRNA (mt-tRNA) mutations that hinder tRNA modifications cause mitochondrial dysfunction and maternally inherited diabetes (19). Intronic polymorphisms in *CDKAL1* are associated with type 2 diabetes (T2D) risk and reduced insulin secretion (20–22). CDKAL1 catalyzes the 2-methylthio (ms^2) modification of N^6-threonyl carbamoyl adenosine (t^6A) in position 37 of $tRNA^{Lys}_{(UUU)}$ (23), an essential modification to prevent codon misreading. In pancreatic β-cells, CDKAL1 deficiency and reduced $tRNA^{Lys}_{(UUU)}$ ms^2 affect lysine incorporation into proinsulin and impair proinsulin processing, leading to endoplasmic reticulum (ER) stress and glucose intolerance in mice (23). Missense mutations in *TRMT10A* lead to early-onset diabetes, microcephaly and intellectual disability (24–29). TRMT10A is the homologue of yeast Trm10, a methyltransferase that methylates guanosine at position 9 (m^1G_9) of selected tRNA species (30,31). TRMT10A is a nuclear protein, ubiquitously expressed but enriched in pancreatic islets and brain, the two main tissues affected in patients. We showed that TRMT10A deficiency sensitizes β-cells to apoptosis (24). *In vitro* methylation assays using recombinant human TRMT10A suggested that, as Trm10, TRMT10A has m^1G_9 tRNA methyltransferase activity (27,32). Here we set out to elucidate the role of human TRMT10A and identify the molecular mechanisms underlying TRMT10A deficiency-induced β-cell death and diabetes.

MATERIALS AND METHODS

Cell culture

Rat INS-1E cells (kindly provided by Prof. Wollheim, University of Geneva, Switzerland) were cultured in RPMI-1640 medium with GlutaMAX-I (ThermoFisher) and 5% FBS as previously described (33). Human clonal EndoC-βH1 cells (kindly provided by Prof. Scharfmann, Université Paris-Descartes, France) were cultured in low glucose DMEM (ThermoFisher) as described (34,35). The same medium with 2% FBS was used for cell treatment (35). Lymphoblasts were obtained from three healthy individuals, four patients with homozygous *TRMT10A* mutations from two families (24,26) and three heterozygous carriers. Patients PA-1 and 2 and the heterozygous carrier of family 1 had a c.379G>A; p.Arg127Stop mutation in *TRMT10A* (24). Patients PA-3 and -4 and two heterozygous carriers from family 2 had a c.79G>T; p.Glu27Stop mutation (26). Lymphoblasts were cultured in RPMI-1640 medium supplemented with 20% FBS, 100 mU/ml penicillin and 100 mU/ml streptomycin. Human islets from non-diabetic organ donors ($n = 6$, age 60 ± 5 years, body mass index 27 ± 2 kg/m^2) were isolated by collagenase digestion and density gradient purification in Pisa, Italy (36) and cultured, dispersed and transfected as previously described (37). β-cell purity, determined by immunofluorescence, was 44 ± 3%.

Human induced pluripotent stem cell differentiation into β-like cells

Fibroblasts were obtained after informed consent, with approval by the Ethics Committees of the Helsinki and Uusimaa Hospital District (no. 423/13/03/00/08) and the Erasmus Hospital, and reprogrammed into induced pluripotent stem cells (iPSCs) using Sendai Virus technology (38). The control iPSC lines HEL46.11 (CT1) (38) and HEL 115.6 (CT2) were derived from human neonatal foreskin (38) and umbilical cord fibroblasts, respectively. The latter were obtained from an unborn male fetus of 31 weeks diagnosed with a lymphangioma of the face. In this individual, microarray-based comparative genomic hybridization was normal ruling-out large chromosomal rearrangements. The TRMT10A-deficient iPSC line HEL122.2 was derived from adult skin fibroblasts. All iPSC lines were cultured in Matrigel-coated plates (Corning BV, Life Sciences) in E8 medium (Life Technologies) and passaged with 0.5 mM EDTA (Life Technologies) twice per week. For β-cell differentiation we used a modified protocol based on earlier studies (38–40). Briefly, iPSCs were washed once with 0.5 mM EDTA, incubated with Accutase (Capricorn Scientific) for 3–8 min and seeded at 1.5–2.5 million cells/3.5 cm Matrigel-coated wells with E8 medium containing 5 μM ROCK inhibitor (StemCell). The 7-stage differentiation was initiated when cell culture reached confluency, 24 or 48 h after plating. iPSCs were washed once with PBS and cultured with stage 1 differentiation medium. Differentiation continued until the end of stage 4 in Matrigel-coated wells. At the end of this stage the cells were washed twice with 0.5 mM EDTA, detached by 5–10 min incubation with Accutase and spun down for 3 min at 250 RCF. The cells were then resuspended in stage 5 medium, containing 10 μM ROCK inhibitor, at a density of 10 million cells/ml in ultra-low attachment 6-well plates (Corning) and kept in suspension by continuous rotation at 100 rpm in the 5% CO_2 incubator, forming compact aggregates 24 hours after plating. The cells were further cultured in stage 5 medium without ROCK inhibitor. Until day 15 of differentiation medium was freshly prepared and changed daily. From day 16 until the end of the differentiation medium was refreshed every second day. The composition of the media is described in Supplementary Tables S3 and S4.

Embryoid body differentiation

The spontaneous differentiation capacity of control HEL115.6 (CT2) and TRMT10A-deficient HEL122.2 iPSCs was evaluated by *in vitro* embryoid body differentiation. The spontaneous differentiation capacity of control iPSCs HEL46.11 (CT1) has been previously reported (38). For embryoid body differentiation the iPSCs were cultured in E8 until 80% confluency, washed twice with 0.5 mM EDTA and detached by 5 min incubation with

Accutase. The cells were resuspended and plated in ultra-low attachment six-well plate in embryoid body medium (Supplementary Table S5) containing ROCK inhibitor, and kept in suspension by continuous rotation at 100 rpm in the 5% CO_2 incubator. Twenty four hours after plating, the ROCK inhibitor was removed. The embryoid bodies were left to differentiate in suspension for two weeks with medium change every second day. After 2 weeks, the embryoid bodies were plated in eight-well chamber slides, let to attach and outgrow for two more weeks after which the cells were fixed for immunofluorescence.

Cell transfection

For RNA interference, INS-1E, EndoC-βH1 cells and dispersed human islets were transfected overnight with 30 nM control siRNA (Qiagen), not interfering with β-cell function or gene expression (37), or siRNAs targeting rat or human TRMT10A, rat Bim and Bad (41) and human Bim (ThermoFisher). For transfection of tRNA fragments, EndoC-βH1 cells were incubated overnight with 30 nM control siRNA (Qiagen), 5′tiRNA^{Gln} or 5′tRFs^{Gln} in its sense (SS) or antisense (AS) version. The stabilized 5′tRFs^{Gln} AS was used at 120 nM. siRNA, tRFs- and tiRNAs-lipid complexes were formed in Opti-MEM medium and transfected using Lipofectamine RNAiMAX or 2000, respectively (ThermoFisher). siRNA, tiRNAs, tRFs and stabilized 5′tRFs^{Gln} AS sequences and lipofectamine concentrations are provided in Supplementary Tables S6–S8.

Cell treatment and apoptosis assays

iPSC-derived β-like cells were exposed to the synthetic ER stressor thapsigargin (1 μM). The ROS scavengers *N*-acetyl L-cysteine (NAC) and 4,5-dihydroxy-1,3-benzenedisulfonic acid (Tiron) were used at 1 mM and 25 μM, respectively.

Apoptosis was detected by fluorescence microscopy after staining with the DNA binding dyes Hoechst 33342 (5 μg/ml, Sigma Aldrich) and propidium iodide (5 μg/ml, Sigma Aldrich) (24). Cell death was determined in at least 600 cells by two observers, one of them unaware of the experimental conditions. Early and late apoptosis was also assessed by Real time-Glo™ Annexin V apoptosis and necrosis assay (Promega) that uses equimolar ratios of two Annexin-V fusion proteins containing complementary subunits of NanoBiT® Luciferase, and a fluorescent DNA-binding probe. Apoptosis was confirmed by immunofluorescence for cleaved caspase-3, Western blots for cleaved caspase-9, and mitochondrial cytochrome *c* release. The separation of cytosolic and mitochondrial fractions was performed in cytosolic lysis buffer (75 mM NaCl, 1 mM NaH_2PO_4, 8 mM Na_2PO_4, 250 mM sucrose, 21 μg/μl aprotinin, 1 mM PMSF) containing 0.8 μg/μl digitonin (Sigma Aldrich).

RNA extraction

Poly(A)$^+$ RNA was isolated using oligo-dT 25-coated polystyrene Dynabeads (Life Technologies) and used for real-time PCR. For total RNA extraction cells were washed with PBS and lysed in Qiazol. The lysate was then loaded into QIAshredder column to break DNA, and small (<200 nucleotides) and long (>200 nucleotides) RNAs were purified using miRNeasy kit (Qiagen) following the manufacturer's instructions. Small RNAs were used for subsequent applications or tRNA purification. RNA was quantified by nanodrop and quality was evaluated by an Agilent Bioanalyzer (Agilent) using the Small RNA Analysis kit.

tRNA purification

tRNA was purified using NucleoBond Xtra resin (Macherey-Nagel) as described (42). Briefly, small RNAs were mixed with an equal volume of equilibration buffer (50 mM Tris-H_3PO_4 pH 6.3, 15% ethanol, 300 mM KCl), loaded into the NucleoBond column, extensively washed with equilibration buffer and eluted with 100 mM Tris-phosphate pH 6.3, 15% ethanol, 650 mM KCl while monitoring the absorbance at 260 nm was monitored. Fractions corresponding to the peak absorbance were pooled, and tRNAs were precipitated by adding 0.7 volume of isopropanol for 1 h at 4°C, followed by 30 min centrifugation at 20000 RCF at 4°C. The pellet was washed once with 70% ethanol and resuspended in RNA-free water. The integrity of purified tRNA was analyzed by denaturing 15% acrilamide gel.

Retrotranscription and real-time PCR

mRNA and long RNA fractions were reverse transcribed as described (24). Real-time PCR was performed using Rotor-Gene SyBR Green on a Rotor-Gene Q cycler (Qiagen) or using IQ SYBR Green Supermix on a MyiQ2 instrument (Bio-Rad). Standards were prepared in a conventional PCR. Gene expression was calculated as copies/μl using the standard curve approach (24). Expression values were corrected for the reference genes GAPDH or β-actin, which were not modified by the experimental conditions. The primers used for real-time PCR and to prepare the standards are provided in Supplementary Tables S9 and S10.

Assessment of guanosine methylation by high-performance liquid chromatography coupled to tandem mass spectrometry

m^1G was quantified by high-performance liquid chromatography (HPLC) coupled, through electrospray ionization, to tandem mass spectrometry (MS) in total RNA and tRNA from lymphoblasts from control individuals, heterozygous mutations carriers and TRMT10A-deficient patients. RNA samples were digested into single nucleosides by overnight incubation with nuclease P1 (Sigma Aldrich) and alkaline phosphatase treatment as previously described (43). HPLC-tandem MS analyses were performed with an Accela chromatographic system coupled to a triple quadrupole Quantum Ultra apparatus (Thermo Electron SAS) equipped with an HESI electrospray source used in the positive ionization mode. HPLC separation was carried out with a 2 × 150-mm octadecylsilyl silica gel (3-mm particle size) column (Uptisphere Interchim, Montluçon, France) and a 0–20% linear gradient of acetonitrile in 0.1% formic acid over 20 min as the mobile phase. MS detection was performed in the multiple reactions monitoring

mode to obtain high sensitivity and specificity. The transitions used to detect m^1G and parent guanosine (Guo) were 298→166 and 284→168, respectively. Guo was eluted at 13.2 min, whereas retention time of m^1G was 15.7 min. For both m^1G and Guo, quantification was performed by external calibration, and the results are given as the number of m^1G per 1000 Guo.

Radioactive labeling of oligonucleotides

Oligonucleotides used for primer extension assays and DNA probes used in northern blots were 5′-end-labeled using ATP [γ-^{32}P] and T4 polynucleotide kinase (T4 PNK) (ThermoFisher). The labeling reaction was performed by mixing 20 pmol oligonucleotide primers or 200 ng DNA probes with 150 μCi ATP [γ-^{32}P], 2 μl 10× T4 PNK reaction buffer, 10U T4 PNK and DEPC-treated water up to 20 μl. Samples were incubated at 37°C for 1 h, and the reaction was stopped by addition of 5 μl EDTA (0.5 mM pH 8.0) and 2 min heating at 95°C.

Detection of guanosine 9 methylation in tRNAs

The presence of m^1G_9 was examined by primer extension assays in lymphoblast tRNA, as described (31). 1 pmol of [γ-^{32}P]ATP-labeled tRNA-specific primers (sequences are provided in Supplementary Table S11) was annealed to 500 ng of purified tRNAs in the presence of 50 mM Tris–HCl pH 8.3, 30 mM NaCl and 10 mM DTT by 2–3 min denaturation at 95°C followed by slow cool down to 37°C. For the primer extension assays and manual sequencing, 100 ng of annealed tRNA/primers were mixed with 5 mM $MgCl_2$, 1x buffer (GeneCraft), 2.5 U MuLV reverse transcriptase (Applied Biosystems), 1 U RNase inhibitor (Applied Biosystems), 2 mM dNTPs (Eurogentec). Manual sequencing was performed by selective incorporation of chain-terminating dideoxynucleotides (ddNTPs). Four separate reactions (A, C, G and T) were performed by adding 2.5 mM of one of the chain-terminating ddNTP (ddATP, ddCTP, ddGTP or ddTTP), 0.05 mM of the corresponding dNTP (dATP, dCTP, dGTP or dTTP) and 0.1 mM of the other three dNTPs. Primer extension and sequencing reactions were incubated for 1 h at 42°C for reverse transcription. The reactions were stopped by adding 7 μl loading buffer containing 90% formamide, 18.6% EDTA, 0.1% xylene cyanol, 0.1% bromophenol blue and 10% glycerol. The amplicons were separated in 15% polyacrylamide gels containing 4 M urea. The gels were then fixed in 1× TBE containing 10% methanol and 10% ethanol, and autoradiography performed using Amersham Hyperfilm MP (GE Healthcare) with TranScreen HE intensifying screen (Kodak). The films were manually developed using Carestream developer and fixator solutions (Kodak).

For the real-time PCR-based detection of m^1G_9, 40–50 ng small RNAs were annealed with specific reverse primers and reverse transcribed. cDNA was then used as template in real-time PCR using the primer combinations (Fw1 + Rev) and (Fw2 + Rev). In Fw1 primers an overhang sequence was added to the 5′ end to allow the annealing of the primer upstream the G9 in tRNA sequences. As in the primer extension assays, the presence of m^1G_9 blocks reverse transcription generating shorter amplicons. As primer Fw1 targets the 5′ end of the tRNA, in the presence of m^1G_9 no PCR amplification will be obtained using the primer pair Fw1 + Rev. The PCR amplification using primer pair Fw2 + Rev is not altered by the presence or absence of m^1G_9; this pair was used as reference. Primer sequences are provided in Supplementary Table S12. The data analysis was performed using the $2^{-\Delta\Delta Ct}$ method according to the formula:

Calculation for lymphoblasts and iPSC-derived β-like cells:

$$\Delta\Delta Ct = \left(Ct^{(Fw1+Rev)} - Ct^{(Fw2+Rev)}\right)_{\text{Patient or control}} - \left(Ct^{(Fw1+Rev)} - Ct^{(Fw2+Rev)}\right)_{\text{AVG Controls}}$$

where AVG Controls is the average of the ΔCt of two to three controls.

Calculation for TRMT10A-silenced EndoC- βH1 cells:

$$\Delta\Delta Ct = \left(Ct^{(Fw1+Rev)} - Ct^{(Fw2+Rev)}\right)_{\text{siTRMT10A or siCT}} - \left(Ct^{(Fw1+Rev)} - Ct^{(Fw2+Rev)}\right)_{\text{siCT}}$$

In both assays, $tRNA^{His}$ that contains a C in position 9 was used as negative control.

Northern blot

tRNA fragmentation was examined by Northern blot adapting a previously described protocol (44). 10 μg short (<200 bp) RNA was denatured in formamide and run in 15% polyacrylamide-8 M urea gels at 120V for 2–3 h. RNA was transferred to positively charged nylon membrane (ThermoFisher) through electroblot transfer performed at 250 mA for 2 h, followed by 350 mA for 1 h at 4°C in 0.5× TBE. Membranes were crosslinked by short-wave UV light, pre-hybridized for 2 h in hybridization solution (5x SSC, 1x Denhardt's solution (Sigma Aldrich), 7% SDS, 20 mM Na_2PO_4) at 46°C, and then hybridized overnight at 46°C with 10 ng/ml [γ-^{32}P]ATP-labeled tRNA-specific DNA probes complementary to 5′ or 3′ halves of tRNAs. Probe sequences are provided in Supplementary Table S13. Membranes were washed in 2x SSC/0.1% SDS, 1x SSC/0.1% SDS and 0.1x SSC, air-dried and radioactive signal detected by autoradiography.

Quantification of tRFs by real-time PCR

For tRNA fragment quantification total RNA was purified using the miRNeasy kit (Qiagen) as previously described. Before reverse transcription, total RNA samples were subjected to 2′–3′ cyclic phosphate removal and 5′ hydroxyl group phosphorylation using rtStar™ tRF and tiRNA pretreatment Kit (ArrayStar), followed by m^1A, m^3C and m^1G demethylation using recombinant *Escherichia coli* AlkB demethylase, and its mutant AlkB-D135S (45). Plasmids coding for the wild type and mutated enzymes were a gift from Tao Pan (pET30a-AlkB Addgene plasmid #79050, pET30a-AlkB-D135S Addgene plasmid # 79051). The recombinant His-tagged proteins were purified using HisLink protein purification resin (Promega). After treatment, the RNA samples were polyadenylated and reverse transcribed

using miRCURY LNA RT kit (Exiqon) and a poly(T) primer with a 3′ degenerate anchor and a 5′ universal tag. tRNA-derived fragments were quantified by real-time PCR using miRCURY LNA™ SYBER Green PCR Kit (Exiqon), and specific custom-designed miRNA LNA™ PCR primers targeting the first 17 nucleotides of $tRNA^{Gln}$ and hsa-let-7f-5p, used as housekeeping.

tRNA aminoacylation

Ten millon lymphoblasts were incubated for 15 min in 2 ml methionine- or glutamine-free RPMI-1640 supplemented with 10% dialyzed FBS, and then incubated for 10 min in the same medium containing 10 μCi/ml L-[^{35}S]-methionine or L-[3,4–^{3}H(N)]-glutamine at 37°C. Cells were then centrifuged 4 min at 1400 rcf, washed twice with PBS, resuspended in acidic solution (50 mM NaOAc, 10 mM $MgCl_2$, 150 mM NaCl pH 4.5) to preserve amino-acylation, and lysed by the addition of an equal volume acidic phenol:chloroform (Invitrogen). After 2 h, samples were centrifuged at 7000 RCF and the RNA from the aqueous phase precipitated with isopropanol. The pellet was dissolved in the same acidic solution. A fraction of the samples was incubated for 1 h at 37°C with 100 mM Tris–HCl pH 8.9 to ensure the complete deaminoacylation of tRNAs; these samples were used as negative controls. RNA was then re-precipitated with 100% ethanol and the pellet dissolved in 200 μl acid solution. 5 μl was used for RNA quantification by nanodrop and 180 μl used for L-[^{35}S]-methionine or L-[3,4–^{3}H(N)]-glutamine detection in a liquid scintillation analyzer (Packard). tRNA charging was expressed as disintegration per minutes (DPM) divided by RNA content in each sample.

Detection of intracellular reactive oxygen species

ROS were measured with the oxidation-sensitive fluorescent probes dichloro-dihydro-fluorescein diacetate (DCF) and hydroxyphenyl fluorescein (HPF) (ThermoFisher) in cells cultured in poly-lysine-coated black plates. The cells were loaded with 10 μM DCF or HPF for 20 min, washed twice with PBS and measured in a VICTOR multilabel plate reader (PerkinElmer) using excitation and emission spectra of 485 and 535 nm. As a positive control, cells were treated for 2 h with 15 μM menadione.

Measurements of cytosolic H_2O_2 using roGFP2-Orp1

Adenovirus encoding roGFP2-Orp1 under the control of the cytomegalovirus (CMV) promoter was generated and amplified using AdEasy System. The cDNA encoding the probe was inserted in the pShuttle-CMV vector and then recloned into the adenoviral backbone plasmid pAdEasy. The resultant pAd-roGFP2-Orp1 was digested by PacI and transferred in human embryonic kidney (HEK)-293 cells to generate adenovirus particles. Adenovirus was amplified in HEK-293 cells, purified on CsCl gradient, and quantified using the Adeno-X Rapid Titer Kit (Clontech).

INS-1E cells were plated on glass coverslips and transfected with a control siRNA or two different siRNAs targeting rat TRMT10A. Two days after transfection and 48 h before the fluorescence measurements the cells were infected with adenovirus encoding roGFP2-Orp1.

For the dynamic measurements of roGFP2-Orp1, the cell-containing coverslips were mounted in a perifusion chamber maintained at 37°C and placed on a ×40 objective of an inverted microscope. The cells were perifused at a flow rate of ∼1 ml/min with a bicarbonate-buffered Krebs solution containing 120 mM NaCl, 4.8 mM KCl, 2.5 mM $CaCl_2$, 24 mM $NaHCO_3$, 1 g/l BSA (Fraction V, Roche) and 10 mM glucose. This solution was continuously gassed with O_2/CO_2 (94/6) to maintain the pH around 7.4. The fluorescence ratio of roGFP2-Orp1 was measured every 30 s after double excitation, at 400 and 480 nm, and by using an emission filter at 535 nm. The data were normalized to the fluorescence ratio measured at the end of the experiment in the presence of 10 mM DTT (set to 0%) then of 100 μM aldrithiol (set to 100%) to allow comparison between experiments. Cells pretreated for 2 h with 15 μM menadione immediately before the measurements were used as positive control.

Western blot

Cells were lysed in Laemmli buffer, extracts resolved on 10–14% SDS-PAGE and transferred to nitrocellulose membrane (Bio-Rad). Immunoblotting was performed using antibodies against cleaved caspase-9, Bcl-x(L), Bcl-2, cytochrome *c*, CoxIV, α-tubulin and GAPDH (the latter two used as control for protein loading). After incubation with secondary horseradish peroxidase-conjugated antibodies, proteins were detected using SuperSignal West Femto chemiluminescence revealing reagent (ThermoFisher) in a ChemiDoc XRS+ system and quantified by Image Lab software (Bio-Rad). The antibodies and dilutions used are provided in Supplementary Table S14.

Immunofluorescence

Cells were fixed in 4% formaldehyde for 15–20 min, permeabilized with 0.5% triton-X100 for 10 min, blocked with UltraV block (ThermoFisher) for 8–10 min and incubated with primary antibodies diluted in 0.1% Tween in PBS for 3 hours at room temperature or overnight at 4°C. Following incubation for 30 min or 1 h at room temperature with secondary antibodies samples were mounted with Vectashield with DAPI (Vector Laboratories) and covered with glass coverslips. The antibodies and dilutions used are provided in Supplementary Table S14.

Statistical analysis

Data are shown as means ± SE. Individual data points represent independent experiments. Non-normally distributed variables were log-transformed before statistical testing. Comparisons between two groups where done by paired *t*-test, and between three or more groups by one-way ANOVA followed by two-sided Student's paired *t*-test with Bonferroni correction for multiple comparisons. Comparisons between control and TRMT10A-deficient patient cells were made by unpaired *t*-test. Comparisons between control and TRMT10A-deficient iPSC-derived β-like cells were made

by multiple *t*-test using the two-stage step-up method of Benjamini, Krieger and Yekutieli, with false discovery rate of 5%. A P value <0.05 was considered statistically significant.

RESULTS

TRMT10A deficiency leads to decreased tRNA guanosine methylation

Based on homology with yeast Trm10 (30), TRMT10A is predicted to be a tRNA (guanosine) methyltransferase. *In vitro* methylation experiments using recombinant TRMT10A (27,32) have previously shown that TRMT10A has tRNA methyltransferase activity. To evaluate whether TRMT10A deficiency indeed affects tRNA guanosine methylation (m^1G) *in vivo*, we purified small RNAs (<200 nucleotides) from lymphoblasts from three control individuals, four TRMT10A-deficient patients (two with a homozygous c.379G>A; p.Arg127Stop mutation (24) and two with a homozygous c.79G>T; p.Glu27Stop mutation (26)), and three heterozygous *TRMT10A* mutation carriers. The small RNA fraction contained two peaks of tRNAs, a separate microRNA (miRNA) smear region and very little contaminant small ribosomal RNAs (by Agilent Bioanalyzer, Supplementary Figure S1A). m^1G methylation in these small RNAs, was measured by HPLC coupled to tandem MS following complete RNA hydrolysis. In these experiments, an m^1G standard was used to identify the peak corresponding to m^1G in the digested RNA samples (Supplementary Figure S1B). Patient lymphoblasts showed a 50% reduction in m^1G compared to unaffected controls, while a slight increase was observed in heterozygous carriers (Figure 1A and B). To assess whether these m^1G changes occurred in tRNAs, we purified tRNAs (Supplementary Figure S1C) and confirmed that m^1G was 50% lower in patient compared to control lymphoblasts (Figure 1C). These data confirm that TRMT10A is a tRNA methyltransferase in humans, and demonstrate that tRNA methylation is significantly reduced in TRMT10A-deficient cells.

$tRNA^{Gln}$ and $tRNA^{iniMeth}$ are TRMT10A substrates

Yeast Trm10 methylates tRNAs in G_9 (30). In the Modomics database (http://modomics.genesilico.pl/), the two cytosolic human tRNAs for glutamine, $tRNA^{Gln}_{(UUG)}$ and $tRNA^{Gln}_{(CUG)}$ (with minor sequence differences), and $tRNA^{iniMeth}_{(CAU)}$ have a methylated G_9. Since HPLC/MS analysis does not indicate in which position the tRNA is methylated (analysis performed after RNA hydrolysis), we performed primer extension assays (30) to assess whether human TRMT10A methylates these tRNAs in G_9. This approach relies on steric hindrance by m^1G_9 that prevents G–C Watson–Crick base pairing and attenuates primer extension during reverse transcription (Figure 1D). Primer extension assays using oligonucleotides annealing both glutamine tRNAs ($tRNA^{Gln}_{(UUG/CUG)}$) and $tRNA^{IniMeth}_{(CAU)}$, showed longer amplicons in patient lymphoblasts compared to controls (Figure 1E, H). For $tRNA^{Gln}_{(UUG/CUG)}$, sequencing assays in patient and control samples confirmed the identity of the retrotranscribed tRNA (Figure 1F, G) and suggested that in control cells the retrotranscription stops in G_9, while in TRMT10A-deficient cells the tRNA amplification continues towards the end of the tRNA, suggesting that G9 is not methylated. For $tRNA^{IniMeth}_{(CAU)}$ the sequencing experiments failed to accurately assess the identity of the primer extension stop due to poor resolution of the sequencing bands (data not shown). As mentioned above, the Modomics database indicates that m^1G_9 is present in $tRNA^{IniMeth}$ suggesting that the amplification difference observed between patients and controls may be the result of impaired m^1G_9 modification in TRMT10A-deficient samples. $tRNA^{His}_{(GUG)}$, with a cytosine in position 9, was used as negative control in our assays (Figure 1I).

Based on an earlier report (46) we also developed a real-time PCR-based assay to assess m^1G_9 (see schematic representation, Figure 1J) in biological samples. This assay, also based on halted reverse transcription, is a fast and not radioactive approach to determine m^1G_9 modification. Since other modifications such us m^1A, m^3C or N^2,N^2-dimethylguanosine also block reverse transcription (47) and may lead to false interpretation of the results, we interrogated the Modomics database to assess whether these other modifications where present in $tRNA^{Gln}_{(UUG/CUG)}$ and $tRNA^{IniMeth}_{(CAU)}$. m^3C and N^2,N^2-dimethylguanosine were reported to be absent in these tRNAs, while m^1A was present in position 58. To prevent the latter from interfering with the assay, the reverse primers were designed to anneal in this region. In keeping with the primer extension assays, significantly more amplification was seen for $tRNA^{Gln}_{(UUG/CUG)}$ and $tRNA^{IniMeth}_{(CAU)}$ in small RNAs from TRMT10A-deficient patient lymphoblasts compared to controls (Figure 1K, L and Supplementary Table S1), suggestive of reduced m^1G_9 modification. TRMT10A haploinsufficiency did not have a significant impact on m^1G_9 methylation (see heterozygous carrier samples in Figure 1K, L). As expected, there were no differences in $tRNA^{His}_{(GUG)}$ PCR amplification between patient and control lymphoblasts (Figure 1M).

To evaluate the impact of TRMT10A deficiency on tRNA methylation in pancreatic β-cells, we silenced TRMT10A expression in clonal human EndoC-βH1 β-cells (Figure 1N and Supplementary Table S2). As in lymphoblasts, TRMT10A deficiency significantly reduced m^1G_9 in $tRNA^{Gln}_{(UUG/CUG)}$ (Figure 1O and Supplementary Table S2), but the amplification difference was less pronounced than in lymphoblasts. This may be the consequence of the partial and transient TRMT10A knockdown achieved in the silencing experiments (by 70 ± 3%, Figure 1N) compared to a complete and permanent TRMT10A deficiency in patient cells. In keeping with this, TRMT10A-silenced EndoC-βH1 cells showed a non-significant trend for reduced G_9 in $tRNA^{IniMeth}_{(CAU)}$ (Figure 1P). The $tRNA^{His}_{(GUG)}$ amplification profile was not different between control and TRMT10A-silenced cells (Figure 1Q).

Establishment and characterization of iPSC-derived β-like cells

To investigate TRMT10A function in a more patient-relevant β-cell model, we established a 7-stage protocol to

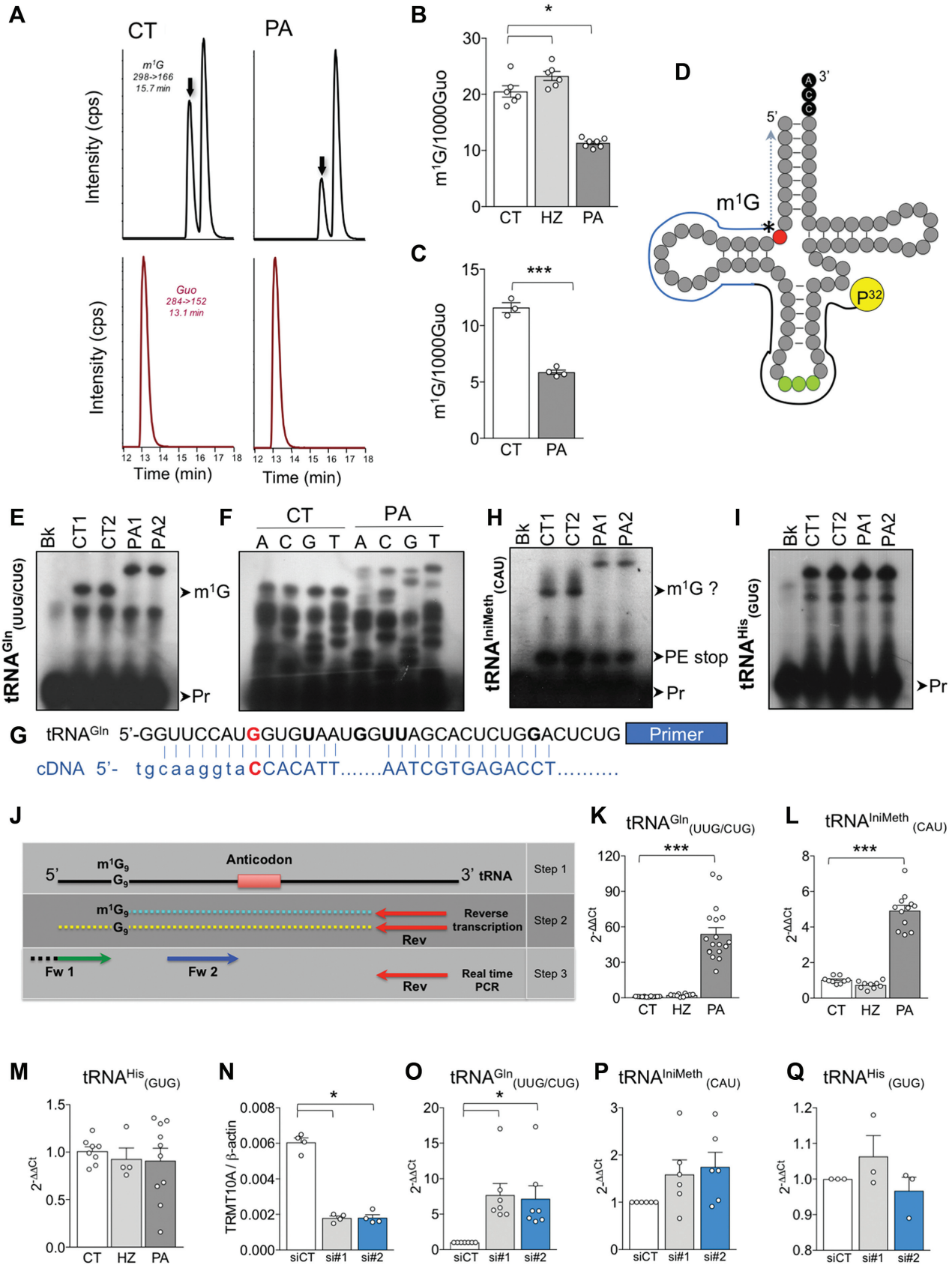

Figure 1. TRMT10A deficiency leads to decreased guanine 9 methylation (m^1G_9). Small RNAs (<200 bp) (**A**, **B**) and tRNAs (**C**) were purified from lymphoblasts from two to four TRMT10A-deficient patients (PA), heterozygous mutation carriers (Hz) and two healthy controls (CT). m^1G modification

differentiate iPSCs into β-like cells (Figure 2A). We used one previously characterized control line (HEL46.11, CT1) (38,48) and generated iPSCs from one TRMT10A patient and an additional healthy control (HEL115.6, CT2). Characterization of the novel TRMT10A and CT2 iPSC lines confirmed expression of pluripotency markers, silencing of exogenous transgenes, and *in vitro* differentiation into the three principal germ layers (endoderm, mesoderm and ectoderm) by embryoid body assay (Supplementary Figure S2A-D). The TRMT10A iPSCs had a normal karyotype (46, XX), and CT2 iPSCs had a 46, XY karyotype with a Y chromosome duplication (Supplementary Figure S2E-F). This was confirmed by band C staining, showing the presence of two centromeres. Since the Y chromosome bears very few loci except for male fertility, the duplication is not expected to affect the present results. The two control and TRMT10A iPSCs differentiated into definitive endoderm expressing SOX17 and subsequently progressed into pancreatic endoderm co-expressing pancreas and duodenal homeobox 1 (PDX1) and NK6 Homeobox 1 (NKX6.1) (Figure 2B). Gene expression across differentiation stages showed a normal developmental pathway with increasing *PDX1* and *NKX6.1* expression, transient expression of *SOX9* and *Neurogenin3* (*NGN3*), followed by induction of its downstream genes *NeuroD1* and *NKX2.2* (Supplementary Figure S3A-F). At the end of the differentiation the islet-like aggregates expressed β-cell-specific insulin and glucagon-like peptide-1 receptor (GLP1R) and α-cell-specific glucagon (Figure 2E, F, Supplementary Figure S3G). Immunofluorescence of stage 7 aggregates showed more C-peptide-positive and less glucagon-positive cells in the control cells compared to TRMT10A patient cells (Figure 2B, C). As in lymphoblasts (24), the patient cells had very low TRMT10A mRNA expression, probably due to mRNA decay (Figure 2D). Having validated the iPSC-derived model, we examined $tRNA^{Gln}$ and $tRNA^{IniMeth}$ G_9 methylation. In keeping with the TRMT10A-deficient lymphoblasts and TRMT10A-silenced EndoC-βH1 cells, the modification of these tRNAs was significantly reduced in TRMT10A-deficient β-like cells; this was already present in earlier stages of differentiation (Figure 2G, H). Collectively, these results identify the cytosolic $tRNA^{Gln}_{(UUG/CUG)}$ and $tRNA^{IniMeth}_{(CAU)}$ as TRMT10A substrates in humans.

m^1G_9 modification is not essential for tRNA aminoacylation

To assess whether TRMT10A deficiency alters tRNA aminoacylation, we measured incorporation of radiolabeled L-[3,4–^{3}H(N)]-glutamine and L-[^{35}S]-methionine into $tRNA^{Meth}$ and $tRNA^{Gln}$ in lymphoblasts from controls and TRMT10A-deficient patients. TRMT10A deficiency did not modify amino acid incorporation (Supplementary Figure S4A and B), suggesting that m^1G_9 is not required for tRNA aminoacylation.

Hypomethylated tRNAs undergo fragmentation

We next examined whether methylation by TRMT10A modulates tRNA fragmentation. For this purpose, we performed Northern blots of TRMT10A-competent and -deficient lymphoblasts using radiolabeled probes complementary to the 5′- or 3′-end of $tRNA^{Gln}$, the 5′-end of $tRNA^{IniMeth}$, and $tRNA^{His}$. $tRNA^{Gln}$ but not $tRNA^{IniMeth}$ was fragmented in TRMT10A-deficient cells, with accumulation of 5′-tRFs of around 22 nucleotides and longer ones probably corresponding to 5′-tiRNAs (Figure 3A, C). Using a 3′-$tRNA^{Gln}$ probe, there was no difference in tRNA fragmentation between patients and controls (Figure 3B), suggesting that the 5′-$tRNA^{Gln}$ fragments are probably the consequence of controlled tRNA fragmentation rather than tRNA degradation. This later process may produce multiple bands that should have been detected by both 5′- and 3′-probes. The absence of increased 3′-$tRNA^{Gln}$ fragments in patient samples is also in good correlation with a tRNA fragmentation process. It has been shown that the stability of the generated tRNA halves can be asymmetric, meaning that in some cases either 5′- or 3′-fragments are detected, the other being rapidly degraded upon generation (49,50). The integrity of the non-TRMT10A target $tRNA^{His}$ was not altered by TRMT10A deficiency (Figure 3D).

To confirm these findings, we quantified 5′-$tRFs^{Gln}$ by real-time PCR (Figure 3E and F) using miRCURY LNA™ Universal RT miRNA PCR system, originally designed to detect miRNAs. Since the presence of m^1A, m^3C and m^1G may interfere with tRF quantification by impairing cDNA synthesis, we pre-treated total RNA with the recombinant demethylases AlkB and AlkB-D135S before reverse transcription. AlkB efficiently demethylates m^1A and m^3C in human tRNAs, while its mutated version AlkB-D135S has enhanced demethylase activity against m^1G (45). The ef-

←

was evaluated by HPLC coupled to MS. (A) Representative MS profiles of small RNAs from one control and one TRMT10A-deficient patient. Upper panel: methylated guanosine (m^1G, arrow), lower panel: unmethylated guanosine (Guo). (B, C) m^1G quantification in number of methylated guanosines per 1000 guanosines (m^1G/1000Guo). **(D, E, H–I)** Assessment of m^1G_9 by primer extension assays in specific tRNAs. **(D)** Schematic representation of the assay. Red circle: G_9; green circles: anticodon; black line: radiolabeled primer. m^1G_9 stops the reverse transcription (blue line, *). In the absence of m^1G_9 the reverse transcription continues towards the 5′ end of the tRNA (blue dotted line). (E, H and I) Primer extension assay for $tRNA^{Gln}$, $tRNA^{IniMeth}$ and $tRNA^{His}$. (**F**) Sequencing lanes for $tRNA^{Gln}$. (**G**) Alignment of $tRNA^{Gln}$ RNA and cDNA sequence, as read in the sequencing assay. Dots represent regions where the sequence could not be assessed. Nucleotides in bold are predicted to be modified in Modomics. G in red: guanosine 9. Bk: primer-only control; Pr, primers; PE stop, primer extension stop. The images are representative of 3–4 independent experiments. (**J**) Schematic representation of the real-time PCR-based assay for m^1G_9 assessment. Small RNA (Step 1) was reverse transcribed using tRNA-specific reverse primers (Step 2). The cDNA was used as template in real-time PCR using the primer combinations (Fw1 + Rev) and (Fw2 + Rev) (Step 3). (**K–M**) Real-time PCR data in lymphoblasts from three controls (CT, $n = 3$–5 independent experiments per individual), three Hz (Hz, $n = 3$ per individual) and four TRMT10A-deficient patients (PA, $n = 2$–3 per individual). (**N–Q**) TRMT10A was silenced in EndoC-βH1 cells using two siRNAs targeting TRMT10A (#1 and #2); cells transfected with a control siRNA were used as control (siCT). **(N)** TRMT10A mRNA expression assessed by real-time PCR and normalized to β-actin. (**O–Q**) Assessment of m^1G_9 by real-time PCR in control and TRMT10A-silenced EndoC-βH1 cells. Data is expressed as $2^{-\Delta\Delta CT}$ that represents relative amplification levels of PA samples versus CT, or siTRMT10A cells versus siCT control cells. Bars show means ± SEM, and data points individual experiments. *$P < 0.05$, siTRMT10A verus siCT; ***$P < 0.001$ PA versus CT by ANOVA followed by *t*-test with Bonferroni correction for multiple comparisons.

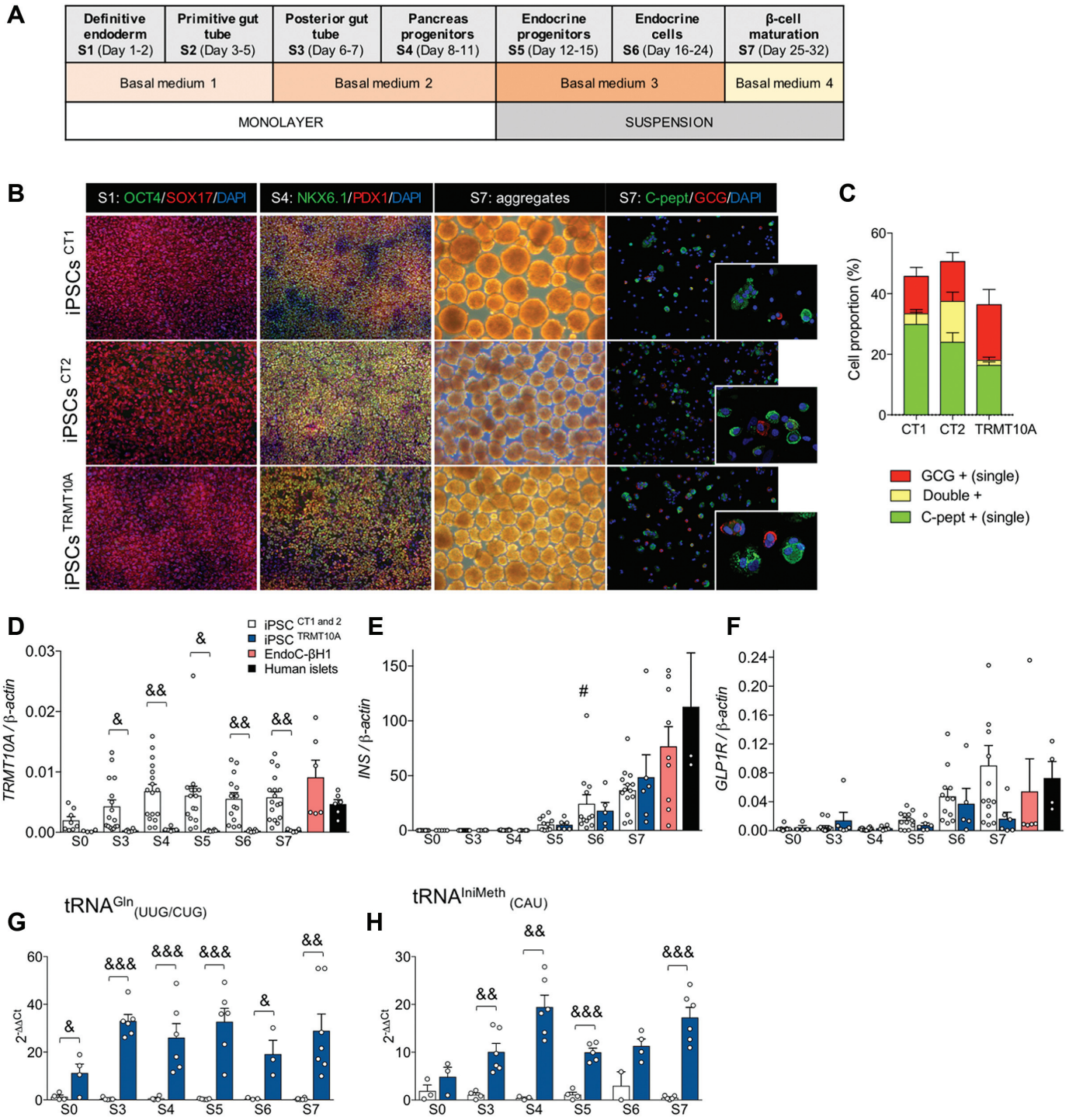

Figure 2. TRMT10A-deficiency leads to impaired tRNA m^1G_9 in iPSC-derived β-like cells. (**A**) Time line of iPSC differentiation into β-like cells. (**B**) Representative immunofluorescence and bright field images of two control (CT1 and CT2) and one TRMT10A-deficient iPSC line during β-cell differentiation. OCT4 and SOX17 were used as pluripotency and definitive endoderm markers, respectively, at the end of stage 1 (S1). NKX6.1 and PDX1 were used as markers of pancreas progenitors (end of stage 4, S4). β- and α-like cells were identified by human C-peptide (C-pept) and glucagon (GCG) staining, respectively. The nuclei were visualized with DAPI. (**C**) Quantification of glucagon (GCG) and C-peptide single positive cells, and CGC + C-peptide double positive cells in the immunofluorescence images. The results are expressed as proportion of total cell number and are means ± SEM of $n = 3$–5 independent experiments. (**D–F**) *TRMT10A*, insulin (*INS*) and glucagon-like peptide-1 receptor (*GLP1R*) mRNA expression assessed by real-time PCR during iPSC differentiation in the two control (CT1 and CT2) and the TRMT10A deficient cell lines, EndoC-βH1 cells and adult human islets. (**G–H**) m^1G_9 in $tRNA^{Gln}$ and $tRNA^{IniMeth}$ measured by real-time PCR. S0: iPSCs, S3–7, Stages 3 to 7. Bars show means ± SEM, and data points independent experiments. $^{\#}P < 0.05$, differential gene expression between a given stage of the differentiation and the preceding one, by ANOVA followed by *t*-test with Bonferroni correction for multiple comparisons. $^{\&}P < 0.05$, $^{\&\&}P < 0.01$; $^{\&\&\&}$Control versus TRMT10A-deficient cells, by multiple *t*-test using the two-stage step-up method of Benjamini, Krieger and Yekutieli, with FDR (*Q*) of 5%.

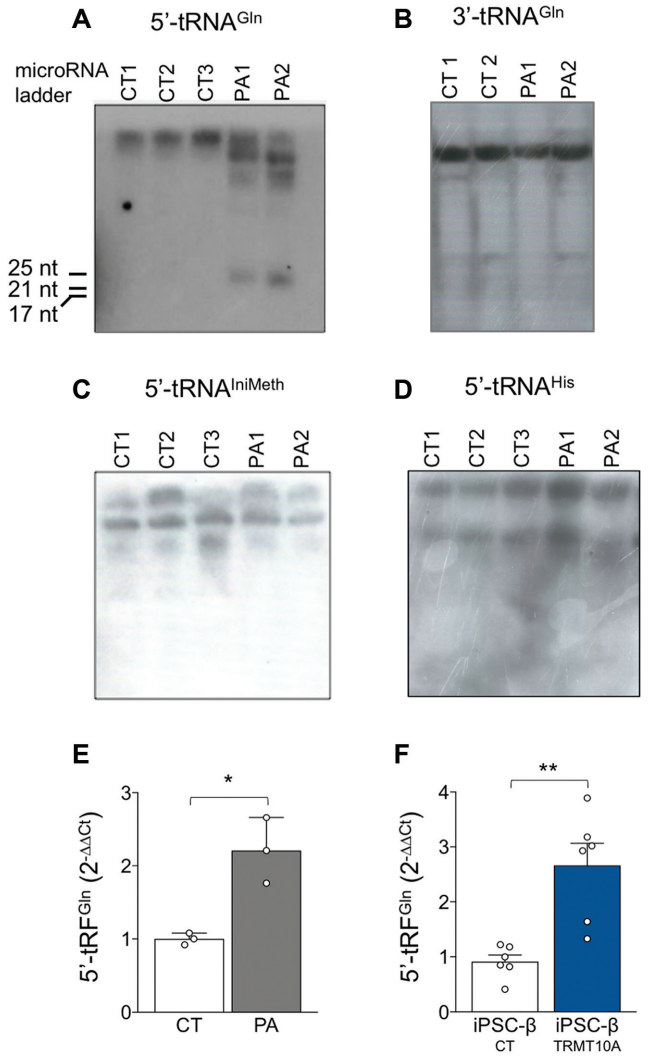

Figure 3. TRMT10A deficiency leads to $tRNA^{Gln}$ fragmentation. tRNA fragmentation was analyzed by Northern blot using radiolabeled probes targeting the 5′ region of $tRNA^{Gln}$, $tRNA^{IniMeth}$ and $tRNA^{His}$ (**A**, **C**, **D**), or the 3′ region of $tRNA^{Gln}$ (**B**). Small 5′-$tRNA^{Gln}$ fragments (tRFs) were detected by real-time PCR (**E**, **F**). $tRNA^{Gln}$ was fragmented in patient samples (PA) compared to controls (CT) evidenced by the accumulation of 5′- (A) but not 3′- (B) -$tRNA^{Gln}$ fragments. No difference in fragmentation was observed for $tRNA^{IniMeth}$ (C) or $tRNA^{His}$ (D). Pictures are representative autoradiographs of 2–3 independent experiments. (E, F) Quantification of 5′-tRF^{Gln} by real time PCR in lymphoblasts from one control and one TRMT10A-deficient patient (D), and iPSC-derived β-like cells from two controls and one TRMT10A-deficient patient (E). miRNA hsa-let-7f-5p was used as reference RNA for normalization. Bars show means ± SEM, and data points independent experiments. $*P < 0.05$, $**P < 0.01$ Control versus TRMT10A-deficient cells, by *t*-test.

fectiveness of the demethylases was confirmed by measuring $tRNA^{Gln}$ m^1G_9 by real-time PCR: untreated patient samples showed enhanced PCR amplification indicating reduced m^1G_9 and this difference was lost by demethylase treatment (Supplementary Figure S4C and D). In agreement with the Northern blots, a significant increase in 5′-$tRFs^{Gln}$ was observed in TRMT10A-deficient lymphoblasts, and in TRMT10A-deficient iPSC-derived β-like cells (Figure 3E and F). Altogether these results demonstrate that hypomethylated $tRNA^{Gln}$ undergoes fragmentation.

Oxidative stress mediates apoptosis in TRMT10A-deficient β-cells

We have previously shown that TRMT10A silencing induces β-cell apoptosis (24). To elucidate the underlying molecular mechanisms, we first silenced TRMT10A in clonal rat INS-1E β-cells using two siRNAs with comparable knockdown efficiency and apoptosis induction (Figure 4A and B). TRMT10A silencing enhanced reactive oxygen species (ROS) production, measured by oxidation of the fluorescent probe DCF (Figure 4C). We also used the more H_2O_2-specific Orp1-roGFP2 (51) and the OH•- and peroxynitrite-specific fluorescent probe HPF (41). Orp1-roGFP2 oxidation was unchanged by TRMT10A silencing (Supplementary Figure S5A), but HPF oxidation was induced, indicative of OH• and peroxynitrite production (Figure 4D). Peroxynitrite is formed by the interaction of superoxide (O_2•) and nitric oxide. No increase in nitric oxide production, measured as accumulated nitrite in the medium (52), was observed in TRMT10A-deficient INS-1E cells (0.45 ± 0.06 μM NO_2^- for siTRMT10A#3, 0.26 ± 0.05 μM NO_2^- for siTRMT10A#4, 0.95 ± 0.34 μM NO_2^- for siCT, $n = 3$).

TRMT10A silencing also induced apoptosis in EndoC-βH1 β-cells, assessed by nuclear dyes and caspase-3 cleavage (Figure 4E–G, Supplementary Figure S5B), and enhanced oxidative stress (HPF oxidation, Figure 4H). To assess whether oxidative stress contributes to the observed β-cell apoptosis, we used the superoxide anion scavenger 4,5-dihydroxy-1,3-benzenedisulfonic acid (Tiron) and the general antioxidant N-acetyl-L-cysteine (NAC). Both compounds abolished β-cell apoptosis induced by TRMT10A deficiency (Figure 4I), demonstrating the important role of oxidative stress.

iPSC-derived β-like cells from controls and a TRMT10A-deficient patient showed indistinguishable basal viability (Figure 4J, untreated), possibly reflecting an adaptive mechanism to constitutive TRMT10A deficiency. In agreement with our previous findings in TRMT10A-silenced clonal β-cells (24), TRMT10A-deficient iPSC-β-like cells showed enhanced sensitivity to apoptosis induced by the ER stressor thapsigargin (Figure 4J–L).

The pro-apoptotic Bcl-2 protein Bim is a key mediator of TRMT10A deficiency-induced β-cell apoptosis

Oxidative stress can induce β-cell death through activation of the intrinsic (mitochondrial) pathway of apoptosis (41). This pathway is controlled in β-cells by anti- and pro-apoptotic Bcl-2 proteins (53) and culminates with mitochondrial permeabilization, cytochrome *c* release, caspase-9 and -3 activation and cell death (54–56). TRMT10A silencing enhanced cytochrome *c* release to the cytosol and induced caspase 9 cleavage in INS-1E (Figure 5A–D) and EndoC-βH1 cells (Figure 5G, H) confirming activation of the intrinsic pathway of apoptosis. TRMT10A deficiency increased mRNA expression of the pro-apoptotic proteins

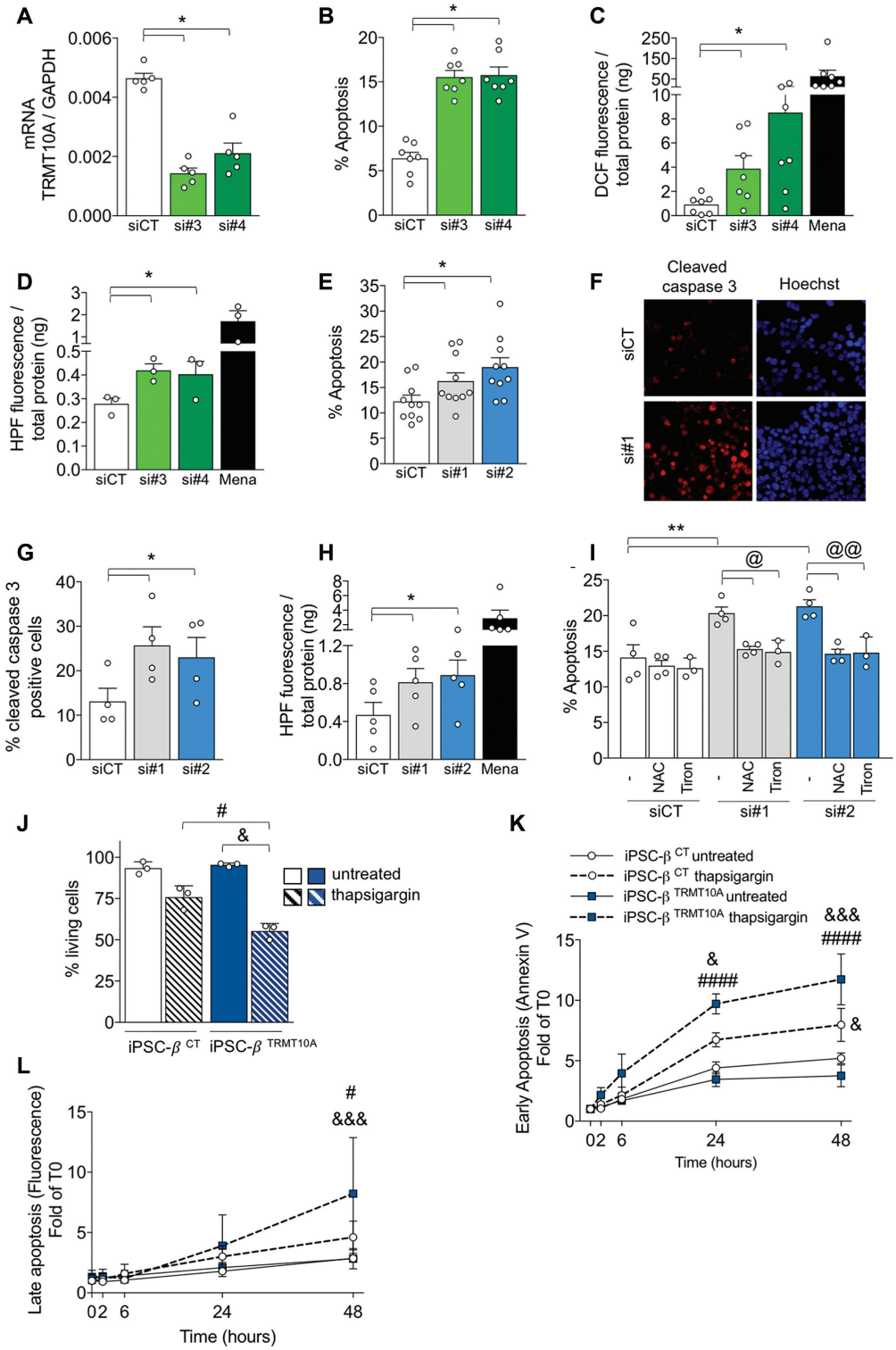

Figure 4. TRMT10A deficiency induces oxidative stress and sensitizes iPSC-derived β-like cells to endoplasmic reticulum stress-induced apoptosis. INS-1E cells (**A–D**) and EndoC-βH1 cells (**E–I**) were transfected with control siRNA (siCT) or two siRNAs targeting rat TRMT10A (#3 and #4) or human TRMT10A (#1 and #2). **(A)** TRMT10A mRNA expression was analyzed by real-time PCR and normalized to GAPDH expression. (B, E, I, J) Apoptosis was examined by Hoechst 33342 and propidium iodide staining. (C, D, H) Oxidative stress was measured by oxidation of the fluorescent probes DCF and HPF. Menadione-treated cells were used as positive control. (F, G) Immunofluorescence of cleaved caspase 3. (F) Representative images of three independent experiments for siCT and siTRMT10A #1 (the full image is provided in Supplementary Figure S5B). (G) Percentage of cleaved caspase 3-positive cells in the immunofluorescence images. (I) Apoptosis of control (siCT) and TRMT10A-deficient cells treated or not (-) with the ROS scavengers Tiron and N-acetyl L-cystein (NAC). (**J**) Viability of control (CT) and TRMT10A-deficient iPSC-β-like cells treated for 48h with the ER stressor thapsigargin (1 μM). (K, L) Time course of thapsigargin-mediated apoptosis in control (CT) and TRMT10A-deficient iPSC-β-like cells. Early (**K**) and late apoptosis (**L**) was assessed by Annexin V-mediated luminescence, and DNA binding dye-mediated fluorescence, respectively. $n = 3$–4 independent experiments. Bars show means ± SEM, and data points independent experiments. $^{*}P < 0.05$, siTRMT10A versus siCT; $^{@}P < 0.05$, $^{@@}P < 0.01$ ROS scavengers versus untreated $^{\&}P < 0.05$, $^{\&\&\&}P < 0.001$, thapsigargin versus untreated; $^{\#}P < 0.05$, $^{\#\#\#}P < 0.001$, iPSC^{CT} versus iPSC^{TRMT10A} by ANOVA followed by *t*-test with Bonferroni correction for multiple comparisons.

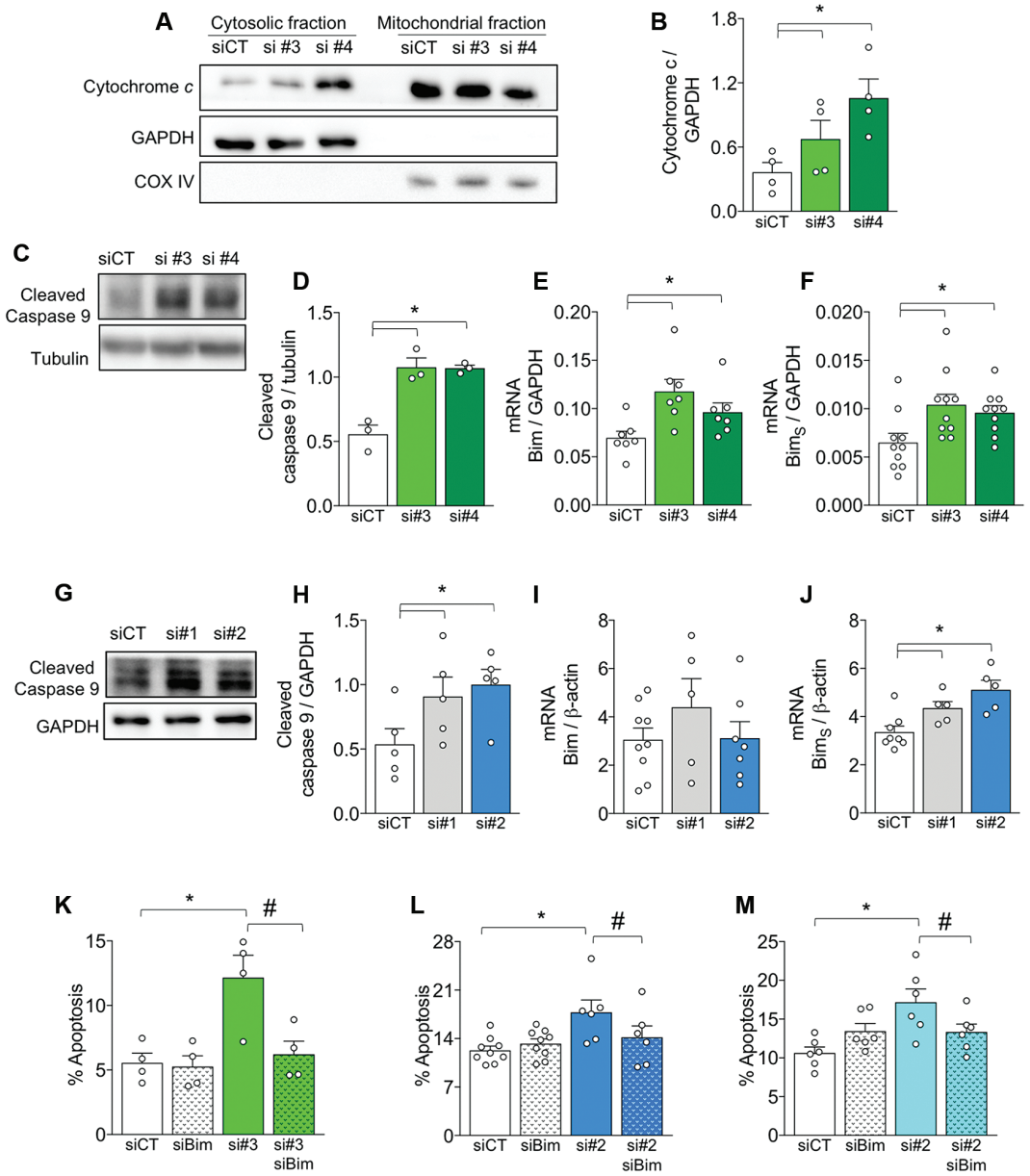

Figure 5. TRMT10A deficiency activates the intrinsic pathway of apoptosis, and induces expression and splicing of the pro-apoptotic protein Bim. INS-1E (**A–F**, **K**), EndoC-βH1 cells (**G–J**, **L**), and dispersed human islets (**M**) were transfected with control siRNA (siCT) or two siRNAs targeting rat (#3 and #4) or human TRMT10A (#1 and #2) alone or in combination with one siRNA targeting rat or human Bim (siBim). (A–D, G–H) Western blots for cytochrome c and cleaved caspase-9. **(A, C, G)** are representative blots and **(B, D, H)** densitometric quantification of the blots. Bim **(E, I)** and Bim small (BimS) (F, J) mRNA expression was evaluated by real-time PCR and normalized to GAPDH or β-actin expression. (**K–M**) apoptosis examined by Hoechst 33342 and propidium iodide staining. Bars show means ± SEM, and data points individual experiments. $^{*}P < 0.05$ siTRMT10A versus siCT, $^{\#}P < 0.05$ TRMT10A versus siTRMT10A-siBim by ANOVA followed by paired *t*-test with Bonferroni correction for multiple comparisons.

Bim (Figure 5E) and Bad (Supplementary Figure S6A) in INS-1E cells, and enhanced Bim splicing into its most pro-apoptotic form Bim small (Bim_S) in rat and human β-cells (Figure 5F, J). TRMT10A silencing did not modify expression of the pro-apoptotic proteins DP5 and PUMA or the pro-survival proteins Bcl-2 and Bcl-x(L) (Supplementary Figure S6B–G). To directly examine the role of Bad or Bim in β-cell apoptosis, we silenced TRMT10A alone or together with Bim or Bad (Supplementary Figure S6H–P). Bim, but not Bad, silencing prevented TRMT10A deficiency-induced apoptosis in clonal rat and human β-cells and in primary human islets (Figure 5K–M, Supplementary Figure S6P), identifying Bim as the key mediator of β-cell death.

5′-tRNA^{Gln} fragments induce β-cell apoptosis

tRNA fragments modulate stress responses and apoptosis (10,16). Since TRMT10A deficiency induces tRNA^{Gln} fragmentation (Figure 3), we examined whether 5′-tRNA^{Gln} fragments mediate β-cell apoptosis. For this purpose, we

transfected TRMT10A-competent EndoC-βH1 cells with synthetic sense (SS) or antisense (AS) 5′-tiRNA^{Gln} and 5′-tRFs^{Gln}. The efficiency of transfection, assessed using fluorescent 5′-tRNA fragments was 25 ± 0% for 5′-tiRNA^{Gln} SS, 25 ± 8% for 5′-tiRNA^{Gln} AS, 16 ± 1% for 5′-tRFs^{Gln} SS, and 16 ± 1% for 5′-tRFs^{Gln} AS (Supplementary Figure S7). 5′-tiRNA^{Gln} SS but not 5′-tiRNA^{Gln} AS induced EndoC-βH1 cell apoptosis, assessed by nuclear staining and caspase 3 cleavage (Figure 6A-C). Transfection with short 5′-tRF^{Gln} SS also induced β-cell apoptosis albeit to a lesser extent (Figure 6D-F). These findings suggest that 5′-tRNA^{Gln} fragments mediate TRMT10A deficiency-induced β-cell death. To confirm this, we transfected TRMT10A-deficient EndoC-βH1 cells with a locked nucleic acid-enhanced antisense oligonucleotide targeting 5′-tRFs^{Gln} (LNA-5′-tRF^{Gln} AS). This molecule with low toxicity and high binding affinity for complementary RNA is resistant to exo- and endonucleases resulting in long-lasting antisense activity. Based on its sequence it is expected to work as a 5′-tRNA^{Gln} fragment inhibitor binding both 5′-tRFs^{Gln} and 5′-tiRNA^{Gln}. This LNA-5′-tRF^{Gln} AS prevented apoptosis induced by TRMT10A deficiency (Figure 6G), supporting the role of 5′-tRNA^{Gln} fragments in β-cell apoptosis.

DISCUSSION

An increasing body of evidence associates mutations in tRNAs or tRNA modifying enzymes with human disease (18). So far no human disease has been linked to cytosolic tRNA mutations, probably due to the presence of multiple paralogs of cytosolic tRNA-encoding genes (57). In contrast, a wide variety of disease-causing mutations in mt-tRNA genes have been described (18). These mitochondrial mutations affect high energy-consuming tissues such as muscle, nervous system and β-cells. Some are associated with maternally inherited diabetes and deafness (19,58–62), resulting in hypomodified mt-tRNAs with impaired function and stability, e.g. m.14692A>G that reduces mt-tRNA^{Glu} pseudouridination at position 55, resulting in tRNA degradation. This affects translation of mitochondrial-encoded glutamic acid-rich proteins such as subunits of respiratory complex I and IV leading to mitochondrial dysfunction (19). Mutations in mitochondrial, cytosolic and nuclear- tRNA-modifying enzymes lead to tRNA hypomodifications and disease. Recessive mutations in *TRMT10C,* coding for the mitochondrial tRNA-methyltransferase MRPP1, cause hypotonia, deafness, elevated lactate levels and premature death (63). MRPP1 and MRPP2 form a stable complex with m^{1}R$_9$ tRNA methyltransferase activity that methylates mt-tRNAs in either G or A in position 9 (32). These two proteins associate with MRPP3, forming the RNase P complex responsible for the 5′ cleavage of mt-tRNAs (64). TRMT10C mutations, leading to reduced MRPP1 levels, impair mt-tRNA processing and induce respiratory chain dysfunction (63). Mutations in *TRIT1*, a tRNA isopentenyltransferase responsible for i^{6}A modification at position 37 of selected mitochondrial tRNAs, cause microcephaly, epilepsy and diabetes (65). Polymorphisms in the cytosolic tRNA modifying enzyme *CDKAL1* are associated with increased T2D risk and reduced insulin secretion (20–23, 66), while non-sense mutations in *TRMT10A*, a nuclear tRNA methyltransferase, cause young-onset diabetes and microcephaly (24–28). The last three examples, associating mutations in mitochondrial, cytosolic and nuclear tRNA-modifying enzymes with diabetes point to a particularly sensitivity of pancreatic β-cells to tRNA hypomodifications.

A previous study using *in vitro* methylation assays with recombinant TRMT10A identified yeast tRNA$^{Gly}_{(GCC)}$ and tRNA$^{Val}_{(UAC)}$ as TRMT10A substrates (31). Here, we confirm the role of TRMT10A as a human m^{1}G$_9$ tRNA methyltransferase, and identify tRNA$^{Gln}_{(UUG/CUG)}$ and tRNA$^{iniMeth}_{(CAU)}$ as TRMT10A substrates. The real-time PCR assays showed that the amplification difference between patients and controls was more pronounced for tRNA$^{Gln}_{(UUG/CUG)}$ than tRNA$^{IniMeth}_{(CAU)}$. This may be the consequence of different amplification efficiencies by the primer sets. Indeed, the presently used real-time PCR approach is a convenient tool to detect differences in tRNA modification between patients and controls, but it is less reliable to assess the abundance of m^{1}G$_9$ modification in a particular tRNA compared to others.

Reduced tRNA modifications can negatively impact tRNA aminoacylation (2) but this was not the case for hypomethylated tRNA$^{Gln}_{(UUG/CUG)}$ and tRNA$^{IniMeth}_{(CAU)}$. Impaired tRNA modifications can also affect tRNA stability (2). Trm10 deficiency in yeast leads to tRNA destabilization and rapid tRNA decay evidenced by complete cell growth arrest in mutants upon exposition to 5-fluoroacyl at 38°C (67). Our data suggest that TRMT10A deficiency in humans leads to tRNA$^{Gln}_{(UUG/CUG)}$ fragmentation, with accumulation of 5′- but not 3′-tRNA fragments, suggesting that m^{1}G$_9$ prevents tRNA^{Gln} cleavage. However, changes in tRNA processing and/or tRNA decay cannot be formally excluded. tRNA fragments are a new class of small non-coding RNAs that modulate a number of cellular processes (15,68). The cleavage by angiogenin of tRNAs into tiRNAs is stress-mediated, but little is known about the biogenesis of tRFs. It has been demonstrated that modification of tRNA nucleotides may induce or prevent tRNA cleavage (15). Deficiency of the cytosine tRNA methyltransferases Nsun2 and Dnmt2 induces angiogenin-mediated tiRNAs (16,69). We speculate that the absence of m^{1}G$_9$ renders tRNA^{Gln} prone to enzymatic cleavage, however, further studies are required to unequivocally ascertain whether tRNA^{Gln} fragmentation under TRMT10A deficiency is indeed mediated by angiogenin, Dicer, or other RNA processing enzymes. tRFs may target the 3′ UTR of specific mRNAs and repress their translation (70,71), and/or they may bind complementary RNAs and form duplexes that the canonical miRNA machinery recognizes and cleaves (68,72). Some 5′-tiRNAs were shown to facilitate assembly of stress granules leading to translational inhibition (11,73). In mammals, a 19-nucleotide-long 5′-tRF^{Gln} represses the translation of a subset of mRNAs (74). TRMT10A silencing in rat β-cells induced a small increase in total protein synthesis (24) which argues against global translational repression, at least under control condition following TRMT10A deficiency by RNA interference. We cannot rule out the possibility that 5′-tRFs^{Gln} modulate translation

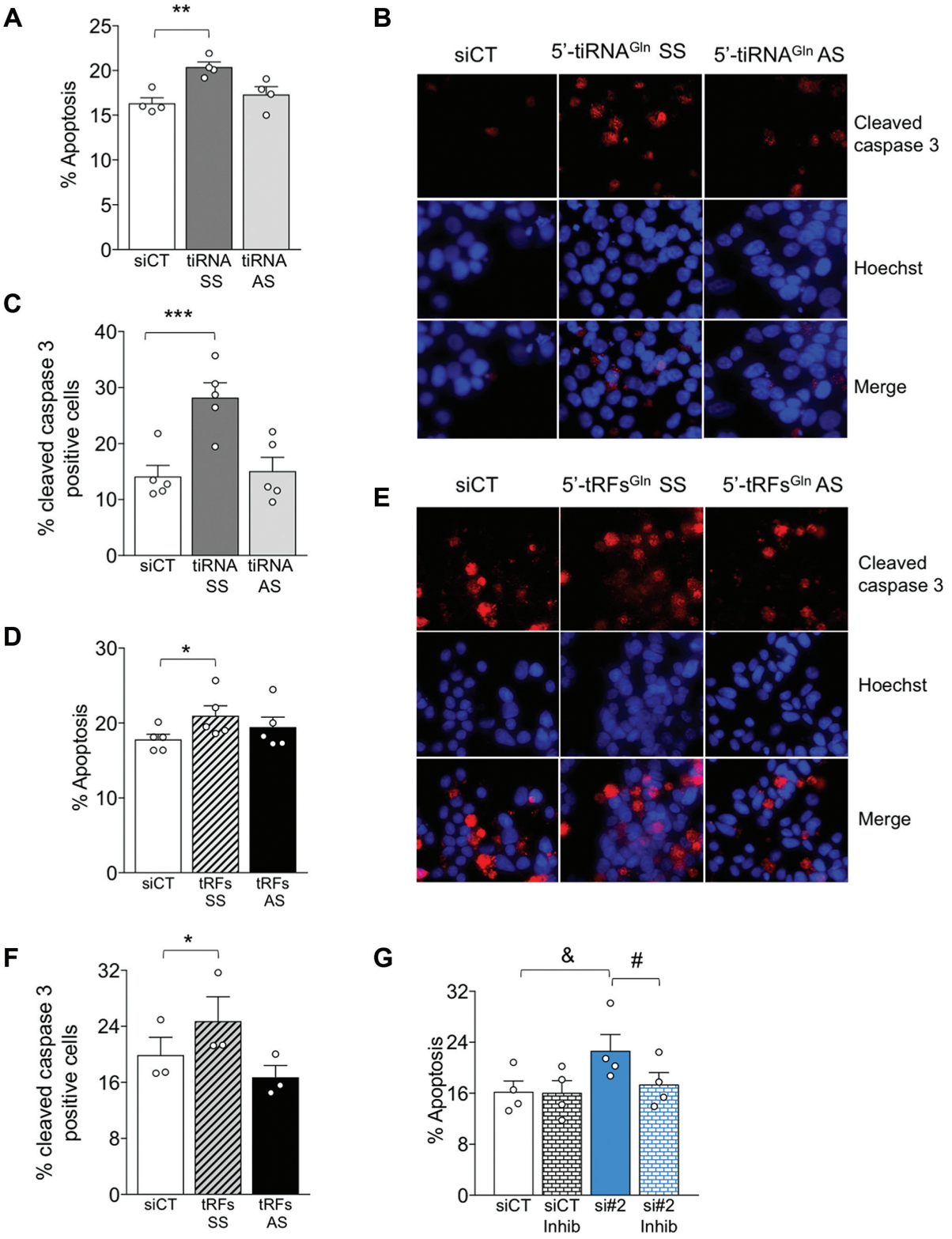

Figure 6. 5′-tiRNA^{Gln} and 5′-tRFs^{Gln} induce apoptosis in EndoC-βH1 cells. TRMT10A competent cells were transfected with a control siRNA (siCT), synthetic oligonucleotides homologous to the 5′-half of tRNA^{Gln} in sense (5′-tiRNA^{Gln} SS) or antisense version (5′-tiRNA^{Gln} AS) (**A–C**), or shorter (18 oligonucleotides) 5′-tRNA^{Gln} fragments in sense (5′-tRFs^{Gln} SS) or antisense version (5′-tRFs^{Gln} AS) (**D–F**). (**G**) EndoC-βH1 cells were transfected with a control siRNA (siCT) or one siRNA targeting TRMT10A (siTRMT10A#2) alone or combined with the tRNA^{Gln} fragment inhibitor LNA-5′-tRF^{Gln} AS. Apoptosis was examined by Hoechst 33342 and propidium iodide staining (A, D, G) and by immunofluorescence of cleaved caspase-3 (B, C, E, F). (B, E) Representative pictures of three to five independent experiments, (C, D) percentage of cleaved caspase-3 positive cells. Results are means ± SEM. Data points represent individual experiments. *$P < 0.05$, **$P < 0.01$, ***$P < 0.001$ 5′-tiRNA^{Gln} SS or 5′-tRF^{Gln} SS versus siCT; $^{\&}P < 0.05$ si#2 versus siCT; $^{\#}P < 0.05$ si#2 versus si#2/siBim, by ANOVA followed by *t*-test with Bonferroni correction for multiple comparisons.

of some mRNAs, or that TRMT10A deficiency represses global protein translation under stress conditions.

The iPSC data do not point to an overt β-cell differentiation defect of TRMT10A-deficient cells, but further work is needed to explore a possible role of TRMT10A in development. TRMT10A patients develop diabetes during adolescence or young adulthood, suggesting they have no major defect in β-cell development. tRNA fragments play a role in cell viability (16). Deficiency in Nsun2, causing microcephaly, leads to impaired cytosine 5 methylation of selected tRNA species and tRNA cleavage; the accumulation of 5′-tiRNAs induces stress responses and neuronal death (16). Here, we show that TRMT10A deficiency induces β-cell oxidative stress and Bim-mediated mitochondrial apoptosis. The apoptosis outcome is phenocopied by introducing sense 5′-tRNA^{Gln} fragments (tiRNAs and tRFs) in TRMT10A-competent β-cells, and a stable 5′-tRF^{Gln} antisense inhibits TRMT10A deficiency-induced apoptosis, indicating that tRNA hypomethylation and consequent cleavage mediate β-cell death. Transfection with 5′-tiRNA^{Gln} SS or 5′-tRFs^{Gln} SS did not induce oxidative stress or Bim expression in EndoC-βH1 cells, possibly related to the low tRNA fragment transfection efficiency (16–25%). tRNA^{iniMeth} was hypomodified but not fragmented in TRMT10A-deficient cells.

In conclusion, we demonstrate here that TRMT10A deficiency leads to tRNA fragmentation as a result of tRNA hypomethylation in guanosine in position 9. This points to a novel mechanism of pancreatic β-cell demise in diabetes. Since TRMT10A deficiency is also associated with microcephaly, our findings may have broader implications, notably related with neuronal loss during brain development.

SUPPLEMENTARY DATA

Supplementary Data are available at NAR Online.

ACKNOWLEDGEMENTS

We thank Isabelle Millard, Michael Pangerl, Ying Cai and Anyishaï Musuaya from the ULB Center for Diabetes Research for excellent technical and experimental support and the cytogenetic department of the Erasmus Hospital for generating lymphoblasts and fibroblasts. We thank Prof. Romano Regazzi and Dr Mustafa Bilal Bayazit for their expert advice on tRNA fragment analysis. We are grateful to the patients and their families for providing blood and skin samples.

Author contributions: C.C., D.L.E., M.C. and M.I-E. contributed to the study design; M.A. and J.-L.R, performed the HPLC-tandem MS analysis; S.T. established the differentiation of iPSC into β-like cells. S.T., S.D., A.S. and N.P. differentiated iPSCs into β-like cells; C.C., E.D.V. and M.I.-E. performed functional experiments. J.-P.D. and J.-C.J. analyzed oxidative stress; C.C., D.L.E., M.C. and M.I.E. analyzed and interpreted the data; D.L.E., M.C., J-C.J., P.M., E.P., T.O., D.B. and M.I.-E. contributed with reagents/materials/analytical tools/expert advice. C.C., M.C. and M.I.-E. wrote the manuscript. M.I.-E. is the guarantor of this work and, as such, had full access to all the data in the study and takes responsibility for the integrity of the data and the accuracy of the data analysis. All authors revised the manuscript and approved the final version.

FUNDING

European Union's Horizon 2020 research and innovation programme, project T2DSystems [667191]; Fonds National de la Recherche Scientifique (F.R.S.-FNRS); Actions de Recherche Concertées de la Communauté Francaise (ARC); FRFS-Welbio, the Innovative Medicines Initiative 2 Joint Undertaking Rhapsody [115881], supported by the European Union's Horizon 2020 research and innovation programme, EFPIA and the Swiss State Secretariat for Education, Research and Innovation (SERI) [16.0097]; Societé Francophone du Diabète (SFD/Novartis); European Foundation for the study of Diabetes (EFSD); Brussels Capital Region-Innoviris; Fondation ULB. E.R.P. is a Wellcome Trust New Investigator [102820/Z/13/Z]. J-C.J . is Research Director of the F.R.S.-FNRS.Funding for open access charge: European Foundation for the Study of Diabetes (EFSD).

Conflict of interest statement. None declared.

REFERENCES

1. Hopper,A.K. and Phizicky,E.M. (2003) tRNA transfers to the limelight. *Genes Dev.*, **17**, 162–180.
2. Phizicky,E.M. and Hopper,A.K. (2010) tRNA biology charges to the front. *Genes Dev.*, **24**, 1832–1860.
3. Agris,P.F. (2004) Decoding the genome: a modified view. *Nucleic Acids Res.*, **32**, 223–238.
4. Agris,P.F., Vendeix,F.A.P. and Graham,W.D. (2007) tRNA's wobble decoding of the Genome: 40 years of modification. *J. Mol. Biol.*, **366**, 1–13.
5. Grosjean,H., de Crécy-Lagard,V. and Marck,C. (2010) Deciphering synonymous codons in the three domains of life: Co-evolution with specific tRNA modification enzymes. *FEBS Lett.*, **584**, 252–264.
6. Motorin,Y. and Helm,M. (2010) tRNA stabilization by modified nucleotides. *Biochemistry*, **49**, 4934–4944.
7. Kadaba,S., Krueger,A., Trice,T., Krecic,A.M., Hinnebusch,A.G. and Anderson,J. (2004) Nuclear surveillance and degradation of hypomodified initiator tRNAMet in S. cerevisiae. *Genes Dev.*, **18**, 1227–1240.
8. Hopper,A.K. (2013) Transfer RNA post-transcriptional processing, turnover, and subcellular dynamics in the yeast Saccharomyces cerevisiae. *Genetics*, **194**, 43–67.
9. Alexandrov,A., Chernyakov,I., Gu,W., Hiley,S.L., Hughes,T.R., Grayhack,E.J. and Phizicky,E.M. (2006) Rapid tRNA decay can result from lack of nonessential modifications. *Mol. Cell*, **21**, 87–96.
10. Anderson,P. and Ivanov,P. (2014) tRNA fragments in human health and disease. *FEBS Lett.*, **588**, 4297–4304.
11. Ivanov,P., Emara,M.M., Villen,J., Gygi,S.P. and Anderson,P. (2011) Angiogenin-induced tRNA fragments inhibit translation initiation. *Mol. Cell*, **43**, 613–623.
12. Yamasaki,S., Ivanov,P., Hu,G.F. and Anderson,P. (2009) Angiogenin cleaves tRNA and promotes stress-induced translational repression. *J. Cell Biol.*, **185**, 35–42.
13. Cole,C., Sobala,A., Lu,C., Thatcher,S.R., Bowman,A., Brown,J.W., Green,P.J., Barton,G.J. and Hutvagner,G. (2009) Filtering of deep sequencing data reveals the existence of abundant Dicer-dependent small RNAs derived from tRNAs. *RNA*, **15**, 2147–2160.
14. Kumar,P., Kuscu,C. and Dutta,A. (2016) Biogenesis and function of transfer RNA-Related fragments (tRFs). *Trends Biochem. Sci.*, **41**, 679–689.
15. Durdevic,Z. and Schaefer,M. (2013) tRNA modifications: necessary for correct tRNA-derived fragments during the recovery from stress? *Bioessays*, **35**, 323–327.
16. Blanco,S., Dietmann,S., Flores,J. V, Hussain,S., Kutter,C., Humphreys,P., Lukk,M., Lombard,P., Treps,L., Popis,M. *et al.*

(2014) Aberrant methylation of tRNAs links cellular stress to neuro-developmental disorders. *EMBO J.*, **33**, 2020–2039.
17. Loss-Morais,G., Waterhouse,P.M. and Margis,R. (2013) Description of plant tRNA-derived RNA fragments (tRFs) associated with argonaute and identification of their putative targets. *Biol Direct*, **8**, 6.
18. Abbott,J.A., Francklyn,C.S. and Robey-Bond,S.M. (2014) Transfer RNA and human disease. *Front. Genet.*, **5**, 158.
19. Wang,M., Liu,H., Zheng,J., Chen,B., Zhou,M., Fan,W., Wang,H., Liang,X., Zhou,X., Eriani,G. *et al.* (2016) A Deafness- and Diabetes-associated tRNA mutation causes deficient pseudouridinylation at position 55 in tRNA ^{Glu} and mitochondrial dysfunction. *J. Biol. Chem.*, **291**, 21029–21041.
20. Saxena,R., Voight,B.F., Lyssenko,V., Burtt,N.P., de Bakker,P.I., Chen,H., Roix,J.J., Kathiresan,S., Hirschhorn,J.N., Daly,M.J. *et al.* (2007) Genome-wide association analysis identifies loci for type 2 diabetes and triglyceride levels. *Science*, **316**, 1331–1336.
21. Chistiakov,D.A., Potapov,V.A., Smetanina,S.A., Bel'chikova,L.N., Suplotova,L.A. and Nosikov,V.V. (2011) The carriage of risk variants of CDKAL1 impairs beta-cell function in both diabetic and non-diabetic patients and reduces response to non-sulfonylurea and sulfonylurea agonists of the pancreatic KATP channel. *Acta Diabetol.*, **48**, 227–235.
22. Dehwah,M.A., Wang,M. and Huang,Q.Y. (2010) CDKAL1 and type 2 diabetes: a global meta-analysis. *Genet. Mol. Res.*, **9**, 1109–1120.
23. Wei,F.Y., Suzuki,T., Watanabe,S., Kimura,S., Kaitsuka,T., Fujimura,A., Matsui,H., Atta,M., Michiue,H., Fontecave,M. *et al.* (2011) Deficit of tRNA(Lys) modification by Cdkal1 causes the development of type 2 diabetes in mice. *J. Clin. Invest.*, **121**, 3598–3608.
24. Igoillo-Esteve,M., Genin,A., Lambert,N., Desir,J., Pirson,I., Abdulkarim,B., Simonis,N., Drielsma,A., Marselli,L., Marchetti,P. *et al.* (2013) tRNA methyltransferase homolog gene TRMT10A mutation in young onset diabetes and primary microcephaly in humans. *PLos Genet.*, **9**, e1003888.
25. Zung,A., Kori,M., Burundukov,E., Ben-Yosef,T., Tatoor,Y. and Granot,E. (2015) Homozygous deletion of TRMT10A as part of a contiguous gene deletion in a syndrome of failure to thrive, delayed puberty, intellectual disability and diabetes mellitus. *Am. J. Med. Genet. A*, **167A**, 3167–3173.
26. Yew,T.W., McCreight,L., Colclough,K., Ellard,S. and Pearson,E.R. (2016) tRNA methyltransferase homologue gene TRMT10A mutation in young adult-onset diabetes with intellectual disability, microcephaly and epilepsy. *Diabet. Med.*, **33**, e21–e25.
27. Gillis,D., Krishnamohan,A., Yaacov,B., Shaag,A., Jackman,J.E. and Elpeleg,O. (2014) TRMT10A dysfunction is associated with abnormalities in glucose homeostasis, short stature and microcephaly. *J. Med. Genet.*, **51**, 581–586.
28. Narayanan,M., Ramsey,K., Grebe,T., Schrauwen,I., Szelinger,S., Huentelman,M., Craig,D. and Narayanan,V. (2015) Case Report: Compound heterozygous nonsense mutations in TRMT10A are associated with microcephaly, delayed development, and periventricular white matter hyperintensities. *F1000Res*, **4**, 912.
29. Shields,B.M., Shepherd,M., Hudson,M., McDonald,T.J., Colclough,K., Peters,J., Knight,B., Hyde,C., Ellard,S., Pearson,E.R. *et al.* (2017) Population-Based assessment of a Biomarker-Based screening pathway to aid diagnosis of monogenic diabetes in Young-Onset patients. *Diabetes Care*, **40**, dc170224.
30. Jackman,J.E., Montange,R.K., Malik,H.S. and Phizicky,E.M. (2003) Identification of the yeast gene encoding the tRNA m1G methyltransferase responsible for modification at position 9. *RNA*, **9**, 574–585.
31. Swinehart,W.E., Henderson,J.C. and Jackman,J.E. (2013) Unexpected expansion of tRNA substrate recognition by the yeast m1G9 methyltransferase Trm10. *RNA*, **19**, 1137–1146.
32. Vilardo,E., Nachbagauer,C., Buzet,A., Taschner,A., Holzmann,J. and Rossmanith,W. (2012) A subcomplex of human mitochondrial RNase P is a bifunctional methyltransferase–extensive moonlighting in mitochondrial tRNA biogenesis. *Nucleic Acids Res.*, **40**, 11583–11593.
33. Asfari,M., Janjic,D., Meda,P., Li,G., Halban,P.A. and Wollheim,C.B. (1992) Establishment of 2-mercaptoethanol-dependent differentiated insulin-secreting cell lines. *Endocrinology*, **130**, 167–178.
34. Ravassard,P., Hazhouz,Y., Pechberty,S., Bricout-Neveu,E., Armanet,M., Czernichow,P. and Scharfmann,R. (2011) A genetically engineered human pancreatic beta cell line exhibiting glucose-inducible insulin secretion. *J. Clin. Invest.*, **121**, 3589–3597.
35. Brozzi,F., Nardelli,T.R., Lopes,M., Millard,I., Barthson,J., Igoillo-Esteve,M., Grieco,F.A., Villate,O., Oliveira,J.M., Casimir,M. *et al.* (2015) Cytokines induce endoplasmic reticulum stress in human, rat and mouse beta cells via different mechanisms. *Diabetologia*, **58**, 2307–2316.
36. Lupi,R., Dotta,F., Marselli,L., Del Guerra,S., Masini,M., Santangelo,C., Patane,G., Boggi,U., Piro,S., Anello,M. *et al.* (2002) Prolonged exposure to free fatty acids has cytostatic and pro-apoptotic effects on human pancreatic islets: evidence that beta-cell death is caspase mediated, partially dependent on ceramide pathway, and Bcl-2 regulated. *Diabetes*, **51**, 1437–1442.
37. Moore,F., Colli,M.L., Cnop,M., Esteve,M.I., Cardozo,A.K., Cunha,D.A., Bugliani,M., Marchetti,P. and Eizirik,D.L. (2009) PTPN2, a candidate gene for type 1 diabetes, modulates interferon-gamma-induced pancreatic β-cell apoptosis. *Diabetes*, **58**, 1283–1291.
38. Saarimäki-Vire,J., Balboa,D., Russell,M.A., Saarikettu,J., Kinnunen,M., Keskitalo,S., Malhi,A., Valensisi,C., Andrus,C., Eurola,S. *et al.* (2017) An activating STAT3 mutation causes neonatal diabetes through premature induction of pancreatic differentiation. *Cell Rep.*, **19**, 281–294.
39. Pagliuca,F.W., Millman,J.R., Gürtler,M., Segel,M., Van Dervort,A., Ryu,J.H., Peterson,Q.P., Greiner,D. and Melton,D.A. (2014) Generation of functional human pancreatic β cells in vitro. *Cell*, **159**, 428–439.
40. Rezania,A., Bruin,J.E., Arora,P., Rubin,A., Batushansky,I., Asadi,A., O'Dwyer,S., Quiskamp,N., Mojibian,M., Albrecht,T. *et al.* (2014) Reversal of diabetes with insulin-producing cells derived in vitro from human pluripotent stem cells. *Nat. Biotechnol.*, **32**, 1121–1133.
41. Igoillo-Esteve,M., Gurgul-Convey,E., Hu,A., Dos Santos,L.R.B., Abdulkarim,B., Chintawar,S., Marselli,L., Marchetti,P., Jonas,J.C., Eizirik,D.L. *et al.* (2015) Unveiling a common mechanism of apoptosis in beta-cells and neurons in Friedreich's ataxia. *Hum. Mol. Genet.*, **24**, 2274–2286.
42. Pierrel,F., Douki,T., Fontecave,M. and Atta,M. (2004) MiaB protein is a bifunctional radical-S-adenosylmethionine enzyme involved in thiolation and methylation of tRNA. *J. Biol. Chem.*, **279**, 47555–47563.
43. Bouvier,D., Labessan,N., Clémancey,M., Latour,J.-M., Ravanat,J.-L., Fontecave,M. and Atta,M. (2014) TtcA a new tRNA-thioltransferase with an Fe-S cluster. *Nucleic Acids Res.*, **42**, 7960–7970.
44. Rio,D.C. (2014) Northern blots for small RNAs and microRNAs. *Cold Spring Harb. Protoc.*, **2014**, 793–797.
45. Zheng,G., Qin,Y., Clark,W.C., Dai,Q., Yi,C., He,C., Lambowitz,A.M. and Pan,T. (2015) Efficient and quantitative high-throughput tRNA sequencing. *Nat. Methods*, **12**, 835–837.
46. Xie,P., Wei,F.-Y.F.-Y., Hirata,S., Kaitsuka,T., Suzuki,T.T., Suzuki,T.T. and Tomizawa,K. (2013) Quantitative PCR measurement of tRNA 2-Methylthio modification for assessing type 2 diabetes risk. *Clin. Chem.*, **59**, 1604–1612.
47. Wilusz,J.E. (2015) Removing roadblocks to deep sequencing of modified RNAs. *Nat. Methods*, **12**, 821–822.
48. Achuta,V.S., Grym,H., Putkonen,N., Louhivuori,V., Kärkkäinen,V., Koistinaho,J., Roybon,L. and Castrén,M.L. (2017) Metabotropic glutamate receptor 5 responses dictate differentiation of neural progenitors to NMDA-responsive cells in fragile X syndrome. *Dev. NeuroBiol.*, **77**, 438–453.
49. Haiser,H.J., Karginov,F. V, Hannon,G.J. and Elliot,M.A. (2008) Developmentally regulated cleavage of tRNAs in the bacterium Streptomyces coelicolor. *Nucleic Acids Res.*, **36**, 732–741.
50. Garcia-Silva,M.R., Frugier,M., Tosar,J.P., Correa-Dominguez,A., Ronalte-Alves,L., Parodi-Talice,A., Rovira,C., Robello,C., Goldenberg,S. and Cayota,A. (2010) A population of tRNA-derived small RNAs is actively produced in Trypanosoma cruzi and recruited to specific cytoplasmic granules. *Mol. Biochem. Parasitol.*, **171**, 64–73.
51. de Souza,A.H., Santos,L.R.B., Roma,L.P., Bensellam,M., Carpinelli,A.R. and Jonas,J.-C. (2017) NADPH oxidase-2 does not contribute to β-cell glucotoxicity in cultured pancreatic islets from C57BL/6J mice. *Mol. Cell. Endocrinol.*, **439**, 354–362.
52. Tonnesen,M.F., Grunnet,L.G., Friberg,J., Cardozo,A.K., Billestrup,N., Eizirik,D.L., Størling,J. and Mandrup-Poulsen,T.

(2009) Inhibition of nuclear factor-κB or bax prevents endoplasmic reticulum stress—but not nitric oxide-mediated apoptosis in INS-1E cells. *Endocrinology*, **150**, 4094–4103.
53. Gurzov,E.N. and Eizirik,D.L. (2011) Bcl-2 proteins in diabetes: mitochondrial pathways of beta-cell death and dysfunction. *Trends Cell Biol.*, **21**, 424–431.
54. Brunelle,J.K. and Letai,A. (2009) Control of mitochondrial apoptosis by the Bcl-2 family. *J. Cell Sci.*, **122**, 437–441.
55. Kim,H., Rafiuddin-Shah,M., Tu,H.C., Jeffers,J.R., Zambetti,G.P., Hsieh,J.J. and Cheng,E.H. (2006) Hierarchical regulation of mitochondrion-dependent apoptosis by BCL-2 subfamilies. *Nat. Cell Biol.*, **8**, 1348–1358.
56. Gross,A., Jockel,J., Wei,M.C. and Korsmeyer,S.J. (1998) Enforced dimerization of BAX results in its translocation, mitochondrial dysfunction and apoptosis. *EMBO J.*, **17**, 3878–3885.
57. Chan,P.P. and Lowe,T.M. (2009) GtRNAdb: a database of transfer RNA genes detected in genomic sequence. *Nucleic Acids Res.*, **37**, D93–D97.
58. van den Ouweland,J.M.W., Lemkes,H.H.P.J., Ruitenbeek,W., Sandkuijl,L.A., de Vijlder,M.F., Struyvenberg,P.A.A., van de Kamp,J.J.P. and Maassen,J.A. (1992) Mutation in mitochondrial tRNALeu(UUR) gene in a large pedigree with maternally transmitted type II diabetes mellitus and deafness. *Nat. Genet.*, **1**, 368–371.
59. Guan,M.X., Enriquez,J.A., Fischel-Ghodsian,N., Puranam,R.S., Lin,C.P., Maw,M.A. and Attardi,G. (1998) The deafness-associated mitochondrial DNA mutation at position 7445, which affects tRNASer(UCN) precursor processing, has long-range effects on NADH dehydrogenase subunit ND6 gene expression. *Mol. Cell. Biol.*, **18**, 5868–5879.
60. Zheng,J., Ji,Y. and Guan,M.-X. (2012) Mitochondrial tRNA mutations associated with deafness. *Mitochondrion*, **12**, 406–413.
61. Suzuki,Y., Suzuki,S., Hinokio,Y., Chiba,M., Atsumi,Y., Hosokawa,K., Shimada,A., Asahina,T. and Matsuoka,K. (1997) Diabetes associated with a novel 3264 mitochondrial tRNA(Leu)(UUR) mutation. *Diabetes Care.*, **20**, 1138–1140.
62. Liu,H., Li,R., Li,W., Wang,M., Ji,J., Zheng,J., Mao,Z., Mo,J.Q., Jiang,P., Lu,J. *et al.* (2015) Maternally inherited diabetes is associated with a homoplasmic T10003C mutation in the mitochondrial tRNAGly gene. *Mitochondrion*, **21**, 49–57.
63. Metodiev,M.D., Thompson,K., Alston,C.L., Morris,A.A.M., He,L., Assouline,Z., Rio,M., Bahi-Buisson,N., Pyle,A., Griffin,H. *et al.* (2016) Recessive mutations in TRMT10C cause defects in mitochondrial RNA processing and multiple respiratory chain deficiencies. *Am. J. Hum. Genet.*, **99**, 246.
64. Holzmann,J., Frank,P., Löffler,E., Bennett,K.L., Gerner,C. and Rossmanith,W. (2008) RNase P without RNA: Identification and functional reconstitution of the human mitochondrial tRNA processing enzyme. *Cell*, **135**, 462–474.
65. Yarham,J.W., Lamichhane,T.N., Pyle,A., Mattijssen,S., Baruffini,E., Bruni,F., Donnini,C., Vassilev,A., He,L., Blakely,E.L. *et al.* (2014) Defective i6A37 modification of mitochondrial and cytosolic tRNAs results from pathogenic mutations in TRIT1 and its substrate tRNA. *PLoS Genet.*, **10**, e1004424.
66. Wei,F.Y. and Tomizawa,K. (2011) Functional loss of Cdkal1, a novel tRNA modification enzyme, causes the development of type 2 diabetes. *Endocr. J.*, **58**, 819–825.
67. Gustavsson,M. and Ronne,H. (2008) Evidence that tRNA modifying enzymes are important in vivo targets for 5-fluorouracil in yeast. *RNA*, **14**, 666–674.
68. Keam,S.P. and Hutvagner,G. (2015) tRNA-Derived fragments (tRFs): emerging new roles for an ancient RNA in the regulation of gene expression. *Life (Basel, Switzerland)*, **5**, 1638–1651.
69. Schaefer,M., Pollex,T., Hanna,K., Tuorto,F., Meusburger,M., Helm,M. and Lyko,F. (2010) RNA methylation by Dnmt2 protects transfer RNAs against stress-induced cleavage. *Genes Dev.*, **24**, 1590–1595.
70. Deng,J., Ptashkin,R.N., Chen,Y., Cheng,Z., Liu,G., Phan,T., Deng,X., Zhou,J., Lee,I., Lee,Y.S. *et al.* (2015) Respiratory syncytial virus utilizes a tRNA fragment to suppress antiviral responses through a novel targeting mechanism. *Mol. Ther.*, **23**, 1622–1629.
71. Maute,R.L., Schneider,C., Sumazin,P., Holmes,A., Califano,A., Basso,K. and Dalla-Favera,R. (2013) tRNA-derived microRNA modulates proliferation and the DNA damage response and is down-regulated in B cell lymphoma. *Proc. Natl. Acad. Sci. U.S.A.*, **110**, 1404–1409.
72. Yeung,M.L., Bennasser,Y., Watashi,K., Le,S.-Y., Houzet,L. and Jeang,K.-T. (2009) Pyrosequencing of small non-coding RNAs in HIV-1 infected cells: evidence for the processing of a viral-cellular double-stranded RNA hybrid. *Nucleic Acids Res.*, **37**, 6575–6586.
73. Schimmel,P. (2017) The emerging complexity of the tRNA world: mammalian tRNAs beyond protein synthesis. *Nat. Rev. Mol. Cell Biol.*, **19**, 45–58.
74. Sobala,A. and Hutvagner,G. (2013) Small RNAs derived from the 5′ end of tRNA can inhibit protein translation in human cells. *RNA Biol.*, **10**, 553–563.